Chapter 1

A Theoretical Description of Thin-Film $Cu(In,Ga)Se_2$ Solar Cell Performance

Leonid A. Kosyachenko

Additional information is available at the end of the chapter

http://dx.doi.org/10.5772/59363

1. Introduction

For a long time, solar cells based on $CuIn_{1-x}Ga_xSe_2$ ($Cu(In,Ga)Se_2$, CIGS), similar to CdTe-based devices, keep a stable position in thin-film photovoltaics as an alternative to solar modules based on mono- and poly-silicon wafers. The I-III-VI CIGS alloy is a solid solution of copper indium diselenide (CIS) and copper gallium diselenide (CGS). This alloy is tolerant in terms of material stability and miscibility in a wide range of x, when the semiconductor bandgap varies continuously from about 1.0 eV for CIS to about 1.65 eV for CGS. Irrespective of the material composition, CIGS is a direct-bandgap semiconductor and strongly absorbs sunlight. Because of its high optical absorption coefficient, a much thinner film is required compared to many other semiconductor materials (1–2 μm is enough to absorb most of the sunlight).

To date, mass production of cost-effective thin-film polycrystalline and monolithically interconnected CIGS-based modules has been achieved by many companies worldwide. Since 2007, one Japanese company Solar Frontier, alone for example, delivered over 1 GW CIGS modules. The CIGS devices demonstrate excellent long-term stability; can be fabricated on lightweight and flexible substrates that are desirable for portable, building-integrated photovoltaics and many other applications when solar panels are used to replace conventional building materials in parts of the roof or facades. It should also be noted that the CIGS modules, in addition to their long-term stability, have shown higher resistance to ionizing radiation compared to crystalline Si and III-V solar cells, i.e., such devices are promising for space application [1].

The energy conversion efficiency of CIGS modules is in the range of 12-15%, but for small area laboratory cells, the efficiency milestone of > 20% was achieved in 2010 [2]. In 2014, Solar Frontier has achieved 20.8% energy conversion efficiency for small area CIGS cells and Zentrum für Sonnenenergie-und Wasserstoff-Forschung Baden-Württemberg (ZSW) shortly

improved the cell efficiency to 20.9% [3,4]. Since the efficiency of CIGS modules lie in the 12-15% range (except for a 16.6 % world record [5]), which is about half of the theoretical limit 28-30%, there are plenty of opportunities to contribute towards the scientific and technological advancement of CIGS PV technology.

The device architecture of CIGS and CdTe solar cells are alike, similar to other p-n heterojuctions. In both cases, the CdS/absorber heterostructure is the key element in determining the electrical and photoelecnric characteristics of the device. In CIGS solar cells, the heterojunction is formed between the p-CIGS and n-CdS. The conductivity of CIGS is determined to a large degree by intrinsic defects, while the n-CdS is doped to a much larger extent by donors. This asymmetric doping causes the space charge region (SCR) to extend much further into the CIGS. As in CdTe solar cell, a thin layer of CdS serves as "window", through which radiation penetrates into the absorber.

The difference between these devices lays in their popular superstrate (CdTe) and substrate (CIGS) configurations. In superstrate configuration devices, the sunlight enters the absorber through the glass substrate and transparent conductive oxide layer (TCO, usually SnO_2:F) while only through the TCO layer (usually ZnO:Al) in substrate configuration. These design features are not of fundamental importance from the point of view of the physical processes taking place, but demand different device fabrication technologies. The physical models used for the interpretation of the CdTe solar cell characteristics has been successfully applied with some modifications to the CIGS devices [6,7].

Based on the above reasoning, in this chapter a detailed analysis of the optical and recombination losses in CIGS devices are presented, which are important causes of poor quantum efficiency (QE), leading to low solar-to-electric energy conversion efficiency in solar cells. A quantitative determination of the losses is presented and some possible pathways to reduce them are identified. Calculations of the optical losses are carried out using the optical constants, refractive indices and extinction coefficients, of the materials used. Equally important are the recombination losses, which are determined using the continuity equation considering the drift and diffusion components of the photocurrent and all possible recombination losses. In order to discuss the influence of the electrical parameters of the heterojunction on the photoelectric conversion efficiency of the device, an analysis of the current-voltage characteristics recorded in dark and under illumination is also included in this chapter. It seems that the analysis of the physical process involved in the photoelectric conversion is useful from a practical point of view since undoubted successes in the development of efficient CIGS solar cells have been achieved mainly empirically [8].

2. Optical constants and related material parameters

Three typical cases, with distinct bandgaps for the CIGS absorber E_g=1.02–1.04 eV (x=0), E_g=1.14–1.16 eV ($x \approx 0.3$) and E_g=1.36–1.38 eV (x=0.6 – 0.65) are considered for the analysis. The absorber with bandgap in the range 1.14-1.16 eV is widely utilized in the industry for the mass

http://dx.doi.org/10.5772/59363

production of solar modules, however, material with bandgap in the range 1.36 – 1.38 eV is promising to achieve the theoretically optimal value for maximum efficiency 28–30%.

Fig. 1 shows the schematic representation of a typical CIGS solar cell architecture, where the notations corresponding to the optical constants n_i and κ_i and the reflection coefficients R_{ij} at the interfaces used in the calculations are indicated.

Photoelectric conversion in these solar cells occurs in the CIGS absorber with a thickness of about 2 μm, while a thin n-type CdS buffer layer (20–50 nm) serves as the heterojunction partner and the window through which the radiation penetrates into the absorber. The Al doped ZnO layer serves as TCO with a thickness of 100–500 nm. Application of an undoped high-resistivity i-ZnO layer with thickness in the range 20–50 nm between TCO and CdS is very common in both substrate and superstrate configuration devices. In efficiency solar cells, an antireflection layer MgF_2, generally of ~ 100 nm thick is also deposited onto the front surface of ZnO.

In the QE calculations of CdS/CIGS cell, one needs to know the optical transmission of the ZnO/CdS structure $T(\lambda)$, which is determined by reflections from the interfaces air/ZnO, ZnO/CdS and CdS/CIGS and absorption in the ZnO and CdS layers. For estimating the transmission $T(\lambda)$, it is necessary to know the refractive indices n_i and extinction coefficients κ_i of ZnO, CdS and CIGS. According to the Fresnel equations, when the light is at near-normal incidence, the reflection coefficients (reflectances) from three interfaces R_{12}, R_{23} and R_{34} (see Fig. 1) can be calculated as

$$R_{ij} = \frac{\left| n_i^* - n_j^* \right|^2}{\left| n_i^* + n_j^* \right|^2} = \frac{(n_i - n_j)^2 + (\kappa_i - \kappa_j)^2}{(n_i + n_j)^2 + (\kappa_i + \kappa_j)^2}, \quad (1)$$

where n_i^* and n_j^* are the refractive indices of the materials, which account for light absorption containing imaginary parts and are written as $n_i^* = n_i - i\kappa_i$ and $n_j^* = n_j - i\kappa_j$.

Fig. 2 shows the spectral dependences of n and κ for ZnO taken from [8] and [10], CdS from [11] and CIGS from [12] (in some cases the extinction coefficient was determined using the relation $\kappa = \alpha\lambda/4\pi$, where α is the absorption coefficient).

It is worth to note the fact that for CIGS, the extinction coefficient in the photon energy range $h\nu < E_g$ ($\lambda > \lambda_g$) has a value of 0.04-0.05, which corresponds to an absorption coefficient $\alpha = 4\pi\kappa/\lambda = (4\text{-}5)\times 10^3$ cm^{-1} [12]. With such values of α, a fairly high efficiency should be obtained for the solar cell, but, in fact, this is not observed. At $\lambda > \lambda_g = hc/E_g$, the quantum efficiency decreases quite rapidly with wavelength up to zero within a range about 120-150 nm above λ_g.

This extended QE response can be explained by the presence of so-called 'tails' of the density of states in the bandgap of the semiconductor with strong doping or/and disordered crystal structure. In this case, the electron wave functions and force fields of impurity atoms overlap,

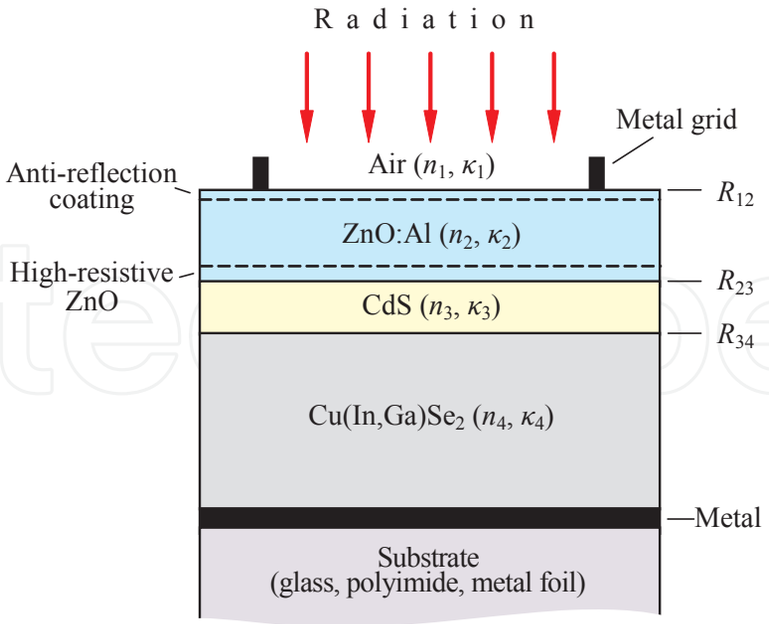

Figure 1. Schematic representation of a typical CIGS solar cell [9].

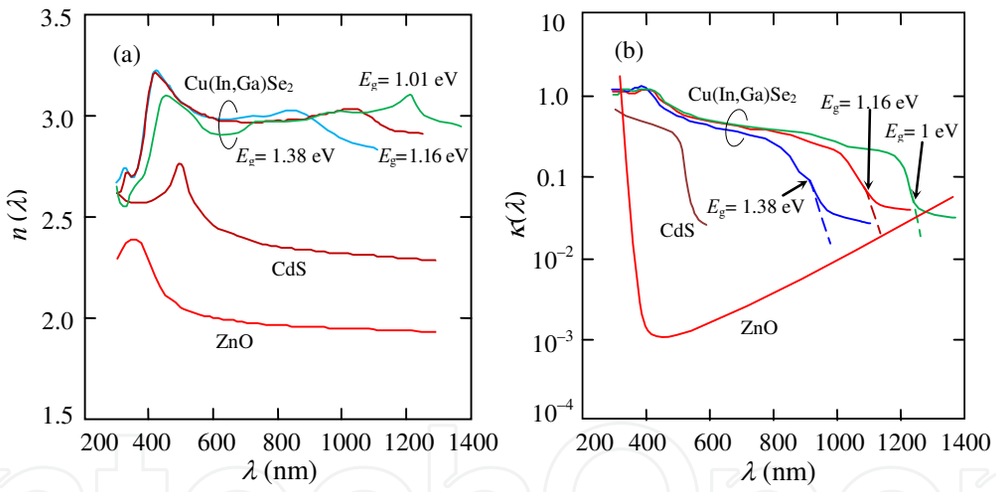

Figure 2. Wavelength dependences of the refractive indices (a) and extinction coefficients (b) of ZnO, CdS, $CuInSe_2$, $CuIn_{0.69}Ga_{0.31}Se_2$ and $CuIn_{0.34}Ga_{0.66}Se_2$.

whereby the discrete impurity levels are broadened and transformed into an impurity band. At a certain critical impurity (defect) concentration, this band joins with the conduction (valence) band, i.e., the tails of the density of states appear. The absorption coefficient in the range of tail depends exponentially on the photon energy, i.e., $\alpha(h\nu) \propto \exp[-(E_g - h\nu)/E_o)$, where E_o is a spectral independent value. Such spectral dependence is sometime called the Urbach rule (E_o can be proportional to kT at sufficiently high T). In this case, in order for the electron to make an interband transition and take part in the formation of the photocurrent, the electron must get the energy, which is equal to or greater than E_g. In the case of the tail

http://dx.doi.org/10.5772/59363

absorption at $h\nu < E_g$ this transition occurs because part of the energy, equal to $h\nu$, electron gets from photon, while the deficit ($E_g - h\nu$) is covered by phonons (the so-called multiphonon transitions). The probability of the multiphonon process decreases exponentially with lowering the $h\nu$, reproducing the spectral curve of photocurrent but with a stronger dependence on $h\nu$ compared with the density of states and the absorption curve (in the tails of state density some of the transitions occur without phonon participation) [13]. It is important to mention that an electron excited due to the absorption of a photon with energy $h\nu < E_g$ takes part in the photocurrent formation just as in the case of absorption of a photon with energy $h\nu \geq E_g$.

Based on the above comments, it is valid to use the $\kappa(\lambda)$ curves of CIGS corrected in the long-wavelength region as shown in Fig. 2b by dashed lines. Anticipating the tail effect, it can be noted that the spectrum at $h\nu < E_g$ makes a relatively small contribution to the photocurrent in solar cells: 1.0 % (0.5 mA/cm^2), 1.1% (0.4 mA/cm^2) and 1.9% (0.6 mA/cm^2) respectively for the absorber bandgaps 1.04, 1.16 and 1.38 eV.

In the range $h\nu \geq E_g$, the absorption coefficient follows the law for a direct-gap semiconductor:

$$\alpha = \alpha_o (h\nu - E_g)^{1/2} / h\nu \ . \tag{2}$$

The above correction of the spectral curves (Fig. 2b) does not exclude the possibility of determining the bandgaps of the samples by using Eq. (2) and the experimental values of α as illustrated in Fig. 3.

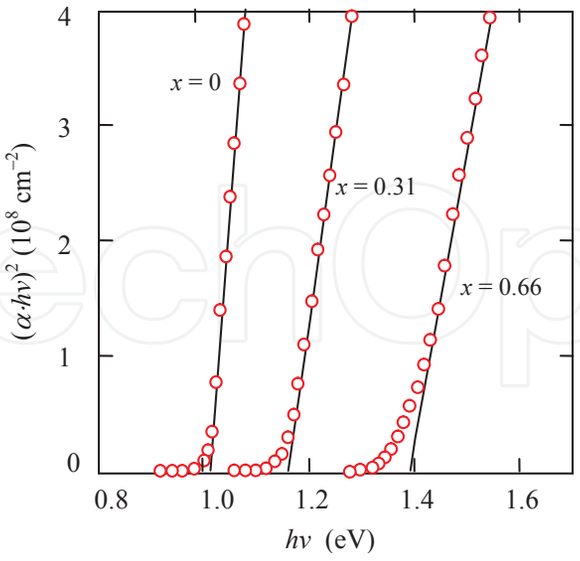

Figure 3. Dependence of the absorption coefficient α of $CuIn_{1-x}Ga_xSe_2$ on the photon energy $h\nu$ in accordance with Eq. (2).

The intercept of the extrapolated straight line portions on the photon energy $h\nu$ axis corresponds to the bandgaps of the discussed materials. The estimated bandgaps are 1.02, 1.16 and

1.38 eV for $CuInSe_2$, $CuIn_{0.69}Ga_{0.31}Se_2$ and $CuIn_{0.34}Ga_{0.66}Se_2$, respectively. The wavelengths corresponding to these bandgaps are indicated on the extinction coefficient data in Fig. 2b by arrows.

3. Optical losses caused by reflection and absorption

The optical transmission $T(\lambda)$ through the multilayer ZnO/CdS/CIGS structure shown in Fig. 1 can be written as

$$T(\lambda) = T_{gr}(1 - R_{12})\exp(-\alpha_2 d_2)(1 - R_{23})\exp(-\alpha_3 d_3)(1 - R_{34}). \quad (3)$$

Here R_{12}, R_{23} and R_{34} are the reflection coefficients at the interfaces air/ZnO, ZnO/CdS and CdS/CIGS respectively, whereas the absorption in ZnO and CdS are represented by $\exp(-\alpha_2 d_2)$ and $\exp(-\alpha_3 d_3)$, where α_2 and α_3, d_2 and d_3 are the absorption coefficients and thicknesses of the ZnO and CdS layers, respectively.

In order to minimize current losses in PV module, thin metal grids are deposited onto the front surface of ZnO, which serve as lateral current collectors. But these grids cause shadowing and a factor T_{gr} is included in Eq. (1) to take care of this effect. In practical modules, the grids are made very narrow and thin such that it shades only about 4–5% of the front area of the ZnO layer. The T_{gr} value can be set to 0.95 without introducing much loss [8].

The effect of an antireflection coating is not considered in Eq. (3), which can significantly reduce the reflectance of the front surface R_{12}. The commonly used antireflection coating for ZnO is MgF_2 which has the refractive index n_{arc} close to the theoretical optimal value $(n_2)^{1/2}$, where n_2 is the refractive index of ZnO. Fig. 4 compares the refractive indices n_{arc}, n_2 and $(n_2)^{1/2}$ in the wavelength region 300 to 1100 nm.

The reflection coefficient R_{arc} of a material with an antireflection coating can be written as [14]:

$$R_{arc} = \frac{r_f^2 + r_b^2 + 2r_f r_b \cos(2\beta)}{1 + r_f^2 r_b^2 + 2r_f r_b \cos(2\beta)}, \quad (4)$$

where r_f and r_b are the Fresnel coefficients, which are the amplitude values of reflectivity from the front and back surfaces of the antireflection material:

$$r_f = \frac{n_{arc} - n_1}{n_{arc} + n_1}, \quad (5)$$

http://dx.doi.org/10.5772/59363

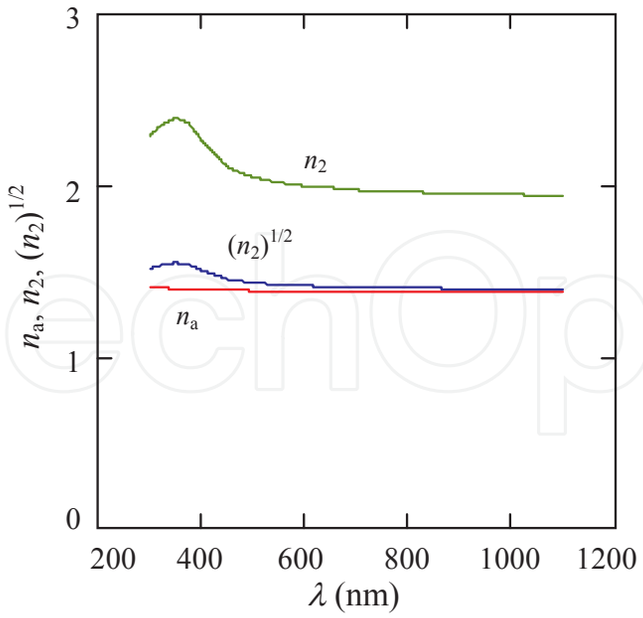

Figure 4. Comparison of the spectral dependences of the refractive indices for ZnO (n_2), MgF_2 (n_{arc}) and $(n_2)^{1/2}$ [9]

$$r_b = \frac{n_2 - n_{arc}}{n_2 + n_{arc}}, \tag{6}$$

and

$$\beta = \frac{2\pi}{\lambda} n_{arc} d_{arc}. \tag{7}$$

Fig. 5a shows a comparison of the reflectance of the bare ZnO surface (curve *1*) and that coated with a 100 nm thick MgF_2 (curve *2*). A comparison of the two curves reveals a significant decrease in reflection in the 500-800 nm region due to the antireflection coating. The observed peak in reflectance at $\lambda < 500$ nm does not produce a significant effect in solar cell performance since the intensity of solar radiation decreases at short wavelength $\lambda < 400$ nm. In addition, the region below 500 nm is dominated by absorption in the CdS film and the ZnO layer. On the contrary, increase in the reflectance at $\lambda > 600$ nm affect the solar cell performance significantly.

So, for taking into account antireflective coating, the reflection coefficient R_{12} in Eq. (3) for the transmission should be replaced by the coefficient R_{arc}, which is determined by Eq. (4):

$$T(\lambda) = T_{gr}(1 - R_{arc})\exp(-\alpha_2 d_2)(1 - R_{23})\exp(-\alpha_3 d_3)(1 - R_{34}). \tag{8}$$

Fig. 5b illustrates the impact of antireflective coating on the transmission property of ZnO/CdS layers in CIGS solar cells.

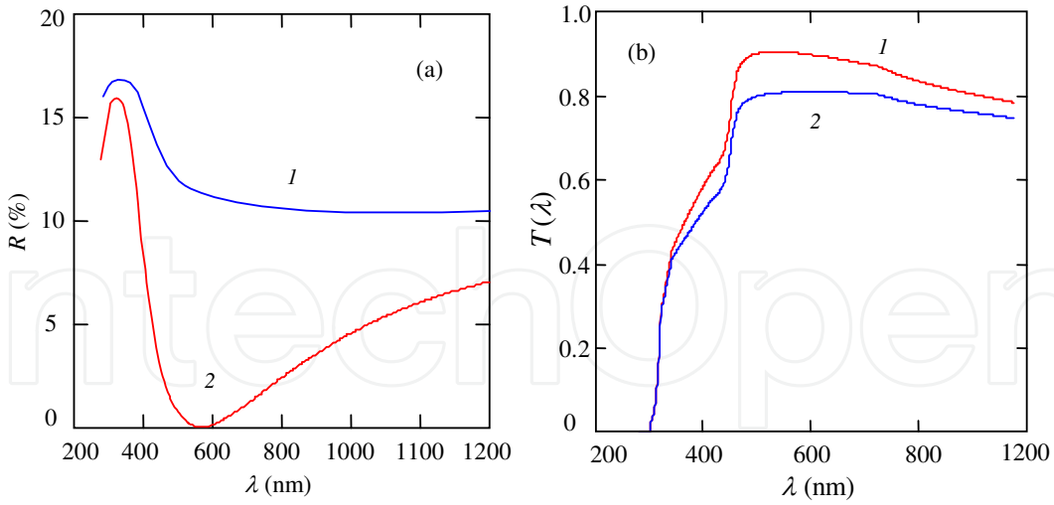

Figure 5. (a) Comparison of the reflectivity of bare ZnO surface (curve *1*) and that coated with MgF_2 (curve *2*). (b) The optical transmission through the ZnO/CdS layers; curve *1* corresponds to ZnO with MgF_2 coating, and curve 2 in the absence of MgF_2 [9].

3.1. Reflection and absorptive losses

From a practical point of view, it is important to assess the various types of losses due to reflections from the interfaces and absorption in the ZnO and CdS layers.

Reflection loss at an interface can be determined using Eq. (8) as the difference between the photon flux that incident on the interface and that passed through it. Absorptive losses can be found from the difference between the photon flux entered the layer and that reached the opposite side.

An estimate of the decrease in solar cells performance due to the optical losses can be obtained by calculating the photocurrent density *J*. The value of *J* for the spectral distribution of AM1.5 global solar radiation is calculated using the Table of International Organization for Standardization ISO 9845-1:1992 [15]. Taking Φ as the incident spectral radiation power density and $h\nu$ the photon energy, then the spectral density of the incident photon flux is $\Phi/h\nu$ and one can write *J* as

$$J = q\sum_i T(\lambda_i)\frac{\Phi_i(\lambda_i)}{h\nu_i}\Delta\lambda_i, \tag{9}$$

where *q* is the electron charge, $\Delta\lambda_i$ is the interval between the neighboring values of λ_i in the ISO table.

Assuming that the solar radiation is negligible for $\lambda < 300$ (> 4.1 eV), the summation in Eq. (9) should be made over the spectral range from λ=300 nm to $\lambda=\lambda_g=hc/E_g$. The corresponding upper limits of the wavelength λ_g for CIGS solar cell with the bandgap of the absorber E_g=1.02–1.04, 1.14–1.16 and 1.36–1.38 eV are ~ 1200, 1080 and 900 nm respectively.

http://dx.doi.org/10.5772/59363

Analyzing the optical losses, we assume that the QE of the solar cell η=1, therefore Eq. (9) does not contain η. If the transmission through ZnO/CdS are also taken as 100%, then the photocurrent density J for the $CuInSe_2$, $CuIn_{0.69}Ga_{0.31}Se_2$ and $CuIn_{0.34}Ga_{0.66}Se_2$ solar cells would be equal to J_o=47.1, 42,0 and 33.7 mA/cm^2, respectively. However, for real situations where there are reflection and absorption losses even with antireflection coating the J value becomes equal to 38.4, 33.9 and 27.5 mA/cm^2 respectively and if there is no antireflection coating the corresponding values are 35.0, 30.8 and 24.8 mA/cm^2. It follows that the antireflection coating increases the photocurrent density J by 3.4, 3.1 and 2.7 mA/cm^2, respectively for the CIGS absorbers discussed above.

It is convenient to report the optical and other types of losses in percentage. Below, all the losses in percentage we will determine relatively to the photocurrent generated by the photon flux incident on the solar cell J_o, i.e., to the above values 47.1, 42,0 and 33.7 mA/cm^2 for the solar cells with the absorber bandgap 1.02–1.04, 1.14–1.16 and 1.36–1.38 eV, respectively. The calculations show that the antireflection coating increases the photocurrent density J by 7.1, 7.4 and 8.0%, for these solar cells, respectively.

Fig. 5a shows that the zero reflectance of ZnO with an antireflection coating takes place at the wavelength of 570 nm for a 100 nm thick layer of MgF_2 that corresponds approximately to the maximum of the solar radiation under the AM1.5 conditions. According to Eq. (4) and (7), the position of the reflectance minimum of the curve *2* depends on the thickness of antireflection coating d_{arc}.

It is interesting to see how the photocurrent density J (which takes into account the spectral distribution of solar radiation) depends on the thickness of the layer d_{arc}. The calculated dependences of decrease in $\Delta J/J_o$ on d_{arc} are shown in Fig. 6 for three samples of the studied solar cells. As seen, the losses are minimal when the thickness of the MgF_2 film is in the range of 105–115 nm that is close to the thickness commonly used of MgF_2 film but the losses become significant when the MgF_2 thickness is below or above the 105-115 nm range. Note that the reflection losses reach the range 9.3–12.4% in the absence of antireflection coating while with coating it is only 1.4–1.9%.

Next the results of calculations of the reflection losses at all interfaces and the absorptive losses in the ZnO and CdS layers are given for solar cells under study.

The losses due to reflection from the front surface of ZnO with an antireflection coating of a 100 nm thick MgF_2 layer in $CuInSe_2$, $CuIn_{0.69}Ga_{0.31}Se_2$ and $CuIn_{0.34}Ga_{0.66}Se_2$ solar cells are equal to 1.9, 1.5 and 1.4%, respectively. Using Eqs. (8) and (9) the calculated values of the reflection loss at the ZnO/CdS interface are 0.9, 0.9 and 1.0% respectively for these solar cells, whereas for the CdS/CIGS interfaces in the three cases the corresponding losses are 1.3, 1.2 and 1.1%, respectively.

Low reflection losses at the interfaces are due to the close values of the optical constants of different layers. This is illustrated in Fig. 7 by plotting the calculated values of the reflectance for ZnO, CdS and $CuIn_{0.33}Ga_{0.67}Se_2$ in the air and in optical contacts with each other. As seen, at the 700 nm region the reflection coefficients at the interfaces (air/MgF_2)/ZnO, ZnO/CdS and CdS/CIGS are 10–17 times smaller than those at the interfaces air/ZnO, air/CdS and air/CIGS.

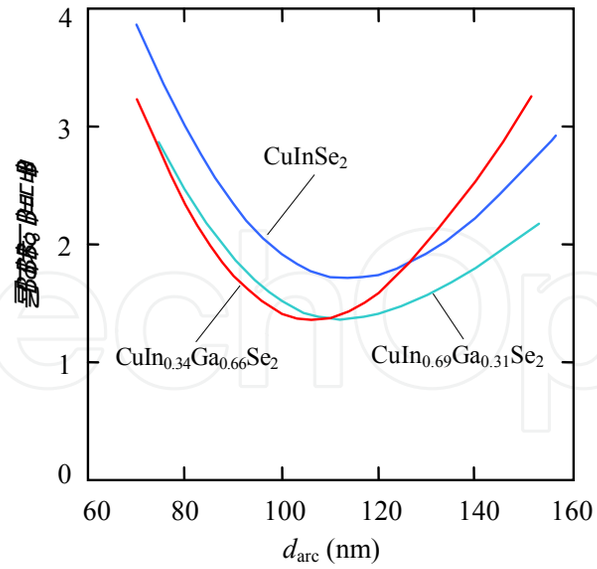

Figure 6. Relation between percentage photocurrent loss and thickness of antireflection coating applied on the ZnO surface for $CuInGaSe_2$, $CuIn_{0.69}Ga_{0.31}Se_2$ and $CuIn_{0.34}Ga_{0.66}Se_2$ solar cells.

The sharp increase in reflectance at λ < 500 nm for the (air/MgF_2)/ZnO interface does not produce a significant effect, which is discussed above.

Absorption losses in the 300 nm thick ZnO and 40 nm thick CdS layers are larger as compared to reflection losses and equal respectively to 2.9 and 5.2% for $CuInSe_2$, 2.2 and 5.6% for $CuIn_{0.69}Ga_{0.31}Se_2$ and 1.9 and 7.7% for $CuIn_{0.34}Ga_{0.66}Se_2$ solar cell. The difference in losses for the three types of samples is due to the difference in their bandgaps.

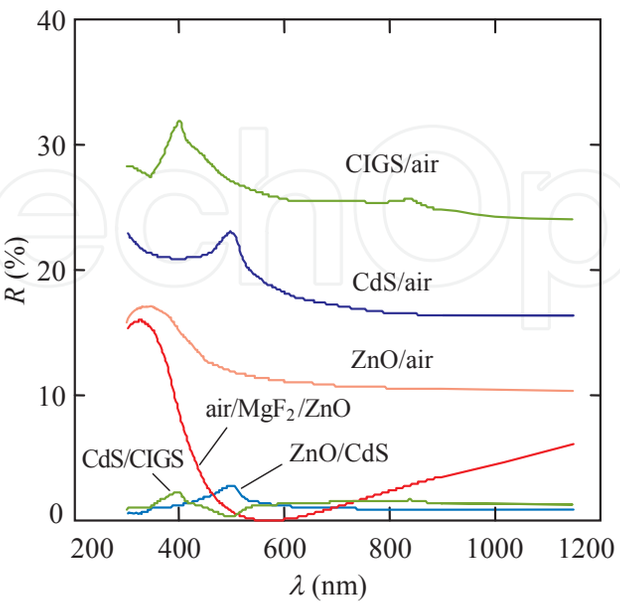

Figure 7. Reflectivity spectra of (MgF_2)ZnO, CdS and $CuIn_{0.34}Ga_{0.66}Se_2$ films in contact with air and other materials [9].

http://dx.doi.org/10.5772/59363

It seems that reflection losses cannot be reduced by virtue of their nature whereas the absorption losses can be reduced by thinning the CdS and ZnO layers. The data in Fig. 8 give some indication of a possible way of lowering these absorption losses. As seen, for d_{CdS}=40 nm, the loss is about 1-3% when the ZnO layer thickness is in the range of 100-500 nm, and when the layer is thinner (100-200 nm) the loss reduces to ~ 1%. The loss due to absorption in CdS layer (Fig. 8b) is higher, 4-5%, even at its lowest thickness of 20-30 nm. It seems that by thinning the CdS and ZnO layers the absorption losses may be limited to 2–3%.

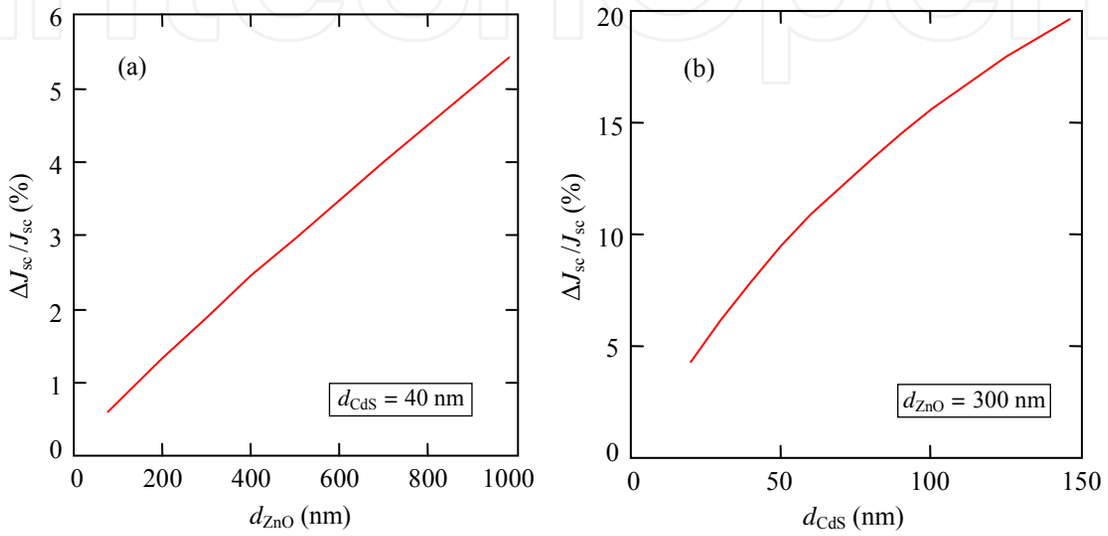

Figure 8. Dependences of the losses caused by absorption in the CdS and ZnO layers on their thicknesses [9].

The calculated values of optical losses along with the corresponding decrease in the photocurrent *J* given in brackets are summarized in Table 1. Note that the calculated data of optical losses are largely in agreement with the results reported in literature, but there are exceptions also. For example, according to our calculations, the reflection losses in $CuIn_{0.69}Ga_{0.31}Se_2$ solar cell (without shading from grid) is equal to 4.0 mA/cm^2 and in reference [8] it amount to 3.8 mA/cm^2, indicating similarity. However, the absorption losses in the CdS film for $CuIn_{0.69}Ga_{0.31}Se_2$ and $CuIn_{0.34}Ga_{0.66}Se_2$ solar cells in our calculations are equal to 2.6–2.9 A/cm^2 and only 0.8 mA/cm^2 in [8]. The losses due to insufficient absorptivity of the CIGS absorber also differ considerably being equal to < 0.1 and 1.9 mA/cm^2, respectively.

Origin of optical losses	Losses in solar cell		
	$CuInSe_2$	$CuIn_{0.69}Ga_{0.31}Se_2$	$CuIn_{0.34}Ga_{0.66}Se_2$
Reflection losses			
Air/ZnO interface with ARC	2.5% (0.8 mA/cm^2)	1.9% (0.6 mA/cm^2)	1.4% (0.5 mA/cm^2)
ZnO/CdS interface	0.9% (0.4 mA/cm^2)	0.9% (0.4 mA/cm^2)	1.0% (0.4 mA/cm^2)
CdS/CIGS interface	1.3% (0.7 mA/cm^2)	1.2% (0.6 mA/cm^2)	1.1% (0.4 mA/cm^2)

Origin of optical losses	Losses in solar cell		
	$CuInSe_2$	$CuIn_{0.69}Ga_{0.31}Se_2$	$CuIn_{0.34}Ga_{0.66}Se_2$
Total reflection losses	4.7% (1.9 mA/cm^2)	4.0% (1.6 mA/cm^2)	3.5% (1.3 mA/cm^2)
Absorption losses			
Absorption in ZnO	2.9% (1.5 mA/cm^2)	2.2% (1.1 mA/cm^2)	1.9% (0.7 mA/cm^2)
Absorption in CdS	5.2% (2.7 mA/cm^2)	5.6% (2.9 mA/cm^2)	7.7% (2.6 mA/cm^2)
Insufficient absorptivity	0.6% (0.1 mA/cm^2)	0.2% (0.1 mA/cm^2)	0.4% (0.1 mA/cm^2)
Total absorption losses	8.1% (4.3 mA/cm^2)	7.8% (4.1 mA/cm^2)	9.6% (3.4 mA/cm^2)
Total optical losses with grid shading	17.4% (9.4 mA/cm^2)	16.0% (9.0 mA/cm^2)	17.5% (7.3 mA/cm^2)

Table 1. Optical and the corresponding photocurrent losses in CIGS solar cells

3.2. Effect of multiple reflection in ZnO and CdS layers

In the calculations outlined in Section 3.1, we omitted the multiple reflections and interference effects in the ZnO and CdS layers, although they occur like those in antireflection coating (oscillations in CIGS are suppressed by strong absorption of the material). It should be noted that the periodic oscillations in the quantum efficiency spectra of the CIGS solar cells, originating from the interference effects, in many cases are not observed. To explain this fact, we calculated the optical transmission of the ZnO/CdS layered structure taking into consideration multiple reflections [9] and using the formula for the double-layer antireflection coatings [16]:

$$R_{\mathrm{dl}} = \frac{r_1^2 + r_2^2 + r_3^2 + r_1^2 r_2^2 r_3^2 + 2r_1 r_2 (1 + r_3^2)\cos(2\,\beta_1) + 2r_2 r_3 (1 + r_1^2)\cos(2\beta_2) + 2r_1 r_3 \cos(2\beta_1 + 2\beta_2)}{1 + r_1^2 r_2^2 + r_2^2 r_3^2 + r_1^2 r_3^2 + 2r_1 r_2 (1 + r_3^2)\cos(2\beta_1) + 2r_2 r_3 (1 + r_1^2)\cos(2\beta_2) + 2r_1 r_3 \cos(2\beta_1 + 2\beta_2)}, \tag{10}$$

where r_1, r_2, and r_3 are the amplitude reflection coefficients for the air/ZnO, ZnO/CdS and CdS/CIGS interfaces:

$$r_1^2 = \frac{(1 - n_2)^2 + (\kappa_2)^2}{(1 + n_2)^2 + (\kappa_2)^2}, \tag{11}$$

$$r_2^2 = \frac{(n_2 - n_3)^2 + (\kappa_2 - \kappa_3)^2}{(n_2 + n_3)^2 + (\kappa_2 + \kappa_3)^2}, \tag{12}$$

$$r_3^2 = \frac{(n_3 - n_4)^2 + (\kappa_3 - \kappa_4)^2}{(n_3 + n_4)^2 + (\kappa_3 + \kappa_4)^2}, \tag{13}$$

n_2, n_3, n_4 and n_2, n_3, n_4 are the refractive indices and extinction coefficients of ZnO, CdS and CIGS, respectively,

$$\beta_1 = \frac{2\pi}{\lambda} n_2 d_{\mathrm{ZnO}}, \tag{14}$$

$$\beta_2 = \frac{2\pi}{\lambda} n_3 d_{\mathrm{CdS}}. \tag{15}$$

Considering a grid contact at the front surface of the ZnO layer and using Eq. (10), one can write the expression for the transmission of the ZnO and CdS layers:

$$T(\lambda) = T_{\mathrm{gr}}(1 - R_{\mathrm{dl}}), \tag{16}$$

where T_{gr} takes into account the shadowing by grid on the front surface of ZnO.

The curve labeled *1* in Fig. 9 shows the calculated transmittance using Eq. (10) and (16) for $CuIn_{0.7}Ga_{0.3}Se_2$ solar cell, and the used parameters are T_{gr}=0.95, d_{ZnO}=300 nm, d_{CdS}=40 nm. The oscillations in the transmission spectrum are clear though the amplitude is small. The small amplitude may be due to the low reflectance from the interfaces since the refractive indices of the contacting layers are close to each other. This is confirmed by the fact that the amplitude of oscillations increases almost twice when the transmission is calculated without antireflective layer on the ZnO front surface.

Eq. (10) describes the oscillations in the reflection spectra due to interference effects in the ZnO and CdS layers, however it does not take into account absorption in these layers. When extinction coefficient κ is small the oscillations due absorption in the layers are visible, but for higher κ the oscillations cannot be observed at all. We can take into account the absorption of solar radiation for one passage in the ZnO and CdS layers by entering in the right side of Eq. (16) the exponential factors appearing in Eqs. (3) and (8):

$$T(\lambda) = T_{\mathrm{gr}}(1 - R_{\mathrm{dl}})\exp(-\alpha_2 d_2)\exp(-\alpha_3 d_3). \tag{17}$$

The results of calculations using Eq. (17) are shown in Fig. 9 as curve *2*. As seen, the oscillation amplitude in the spectral range $\lambda > 500$ nm, where the absorption in ZnO and CdS is weak has remained almost unchanged, but in the range of the interband transitions in CdS at $\lambda < 500$ nm, the amplitude decreased significantly.

The spectrum *3* in Fig. 9 was obtained by using Eq. (3) with $R_{\mathrm{arc}}=R_{12}$, i.e., without considering the multiple reflections in the ZnO and CdS layers. As it is clear from figure, when multiple reflections are considered (spectrum 2) only minor periodic deviations occur from spectrum

3. When calculating the photocurrent density of a solar cell, which is the sum of the current over the entire spectral range, ignoring multiple reflections should not cause significant errors. In fact, photocurrent density calculated using Eqs. (8) and (17) for $T(\lambda)$ shows only a difference less than 0.5% for the studied solar cells.

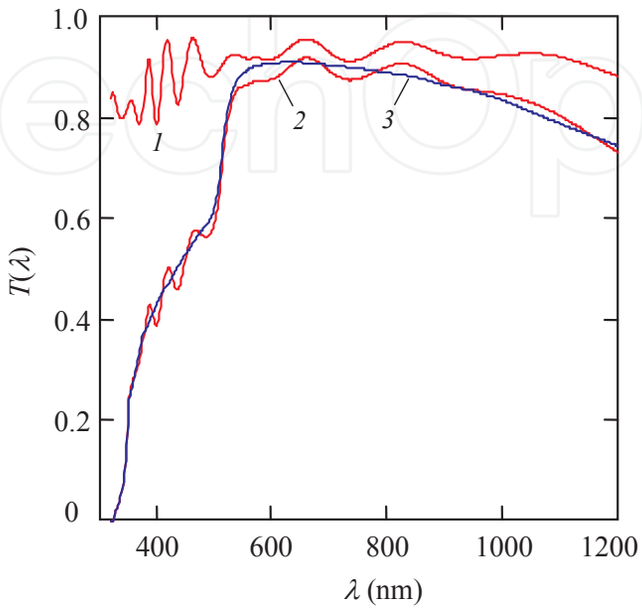

Figure 9. Transmission spectra of ZnO/CdS layers calculated by taking into account the multi-reflections but without considering absorption (line *1*), line 2 is the spectrum when the absorption in the ZnO and CdS layers is taken into account, and line 3 corresponds to case when multi-reflections are neglected [9].

It should also be borne in mind that the Eq. (17) has been deduced for flat, perfect and parallel interfaces air/ZnO, ZnO/CdS and CdS/CIGS. But real interfaces will be far away from the ideal conditions; hence the oscillations in the transmission spectra can be less than 0.5% or even not visible. In contrast, if the interfaces are perfect as mentioned above, the periodic variations in the transmission and photoresponse spectra of the devices will be clear [17].

3.3. Absorptive capacity of the CIGS absorber layer

In the previous sections while discussing the photocurrent, we assumed 100% light-to-electric conversion in the CIGS layer. However, there are losses related to the incomplete absorption of light in this layer. Considering this fact, while estimating the exact values of *integrated* absorptive capacity of the CIGS layer the spectral distribution of solar radiation and absorption coefficient of the material must be taken into account rather than determining the absorptive capacity for one wavelength in the range $h\nu > E_g$.

It should be noted that in the photon energy range from E_g to 4.1 eV electron-hole pairs arise independently of the energy absorbed. In other words, the energy needed for the band to band transition is less than the absorbed energy. So while considering the dependence of the absorptivity of solar radiation power A_Φ (rather than photon flux $A_{h\nu}$) on the thickness of the semiconductor this fact must be considered. For this reason, the number of electron-hole pairs,

http://dx.doi.org/10.5772/59363

and hence the photocurrent generated in the solar cell, is not proportional to the power of solar radiation. Hence, the dependences of A_{hv} and A_{Φ} on the thickness of the semiconductor are different and for calculation of the photocurrent, the absorptivity of photon flux A_{hv} should be used.

The *integrated* absorptive capacity of the semiconductor layer depends on two factors: (i) the spectral distribution of solar radiation, and (ii) the optical transmission of the ZnO and CdS layers that affect the spectral distribution of solar radiation reaching the absorber. With this consideration the integrated absorptivity can be taken as the ratio of the number of photons absorbed in the CIGS layer to the number of photons penetrated through the ZnO and CdS layers [18]:

$$A_{hv}(d) = \frac{\sum_i T(\lambda)\frac{\Phi_i}{h\nu_i}[1-\exp(-\alpha_i d)]\,\Delta\lambda_i}{\sum_i T(\lambda)\frac{\Phi_i}{h\nu_i}\Delta\lambda_i}. \quad (18)$$

Here summation is for the spectral range starting from λ=300 nm and the upper limit depends on the E_g of the material, which corresponds to λ=1200, 1080 or 900 nm respectively for $CuInSe_2$, $CuIn_{0.69}Ga_{0.31}Se_2$ and $CuIn_{0.34}Ga_{0.66}Se_2$ solar cells.

According to Eq. (18) for $CuInSe_2$, $CuIn_{0.69}Ga_{0.31}Se_2$ and $CuIn_{0.34}Ga_{0.66}Se_2$ solar cells, 99.4, 99.6 and 99.8% photon absorption happens for a layer thickness of 2 μm. But with a layer thickness of 1 μm the photon absorptivity values for these solar cells are equal to 97.0, 98.3 and 97.7% respectively, i.e., optical losses become noticeable. On the other hand, in another direct-gap semiconductor CdTe the photon absorptivity of 99.4–99.8% takes place at a thickness of about 30 μm [18].

It should also be borne in mind that CIGS solar cell is a substrate configuration device having metallic substrate as one of the electrodes. This implies that long wavelength radiation with low absorption coefficient can reflect back from the rear surface. In the event of 100% reflectance from the back surface, the absorptivity is the same as for the double thickness of the absorber layer, i.e., the $A_{hv}(d)$ value in such a solar cell can be found by doubling the thickness d in Eq. (18). This means that 99.4–99.8% photon absorption in CIGS takes place at a thickness of 1 μm rather than 2 μm.

4. Recombination losses

Electrons and holes (electron-hole pairs) created as a result of photon absorption in the space charge region (SCR) of CdS/CIGS heterostructure move apart under the influence of the junction built-in voltage. The electrons move towards to CdS side and reach the front metal grid contact after passing through the ZnO layer, while holes move to the neutral part of the CIGS layer and reach the Mo back contact. Not all the photogenerated carriers contribute to

the current; some of the carriers recombine in the SCR before reaching the contacts. Recombination can also occur at the front surface of the absorber contacting with the CdS film. Minority carriers (electrons), which are generated outside the SCR, also take part in the formation of the photocurrent, when electrons reach the SCR as a result of diffusion. This process competes with the recombination of electrons with the majority carriers (holes) in the neutral part of the absorber. Finally, recombination of electrons can occur on the back surface of the absorber, i.e., at the CIGS/metal interface.

For a given thickness of the absorber, the recombination losses depend mostly on the carrier lifetime and the width of the SCR, which in the case of a semiconductor containing both acceptor and donor type impurities are determined by the concentration of uncompensated acceptors $N_a - N_d$. Therefore, investigating the influence of the material parameters on the recombination losses, we will calculate the dependence of photocurrent J on $N_a - N_d$ for several values of carrier lifetimes.

Consideration of the statistics in a nonequilibrium state leads to the conclusion that the lifetimes of electrons τ_{no} and holes τ_{po} in the SCR are approximately equal to the lifetime of minority carriers in heavily doped respectively p-and n-type materials [19]. We assume that in the CIGS solar cell, the absorber is a heavily doped semiconductor (hole concentration is about 10^{15}–10^{16} up to 10^{17} cm^{-3} [8, 21].

The recombination losses can be judged by the value of photocurrent density J using the formula:

$$J = q\sum_i \frac{\Phi_i(\lambda)}{h\nu_i}\, T(\lambda)\eta_{int}(\lambda)\Delta\lambda_i, \tag{19}$$

where $T(\lambda)$ is the optical transmission of the ZnO and CdS layers, and $\eta_{int}(\lambda)$ is the internal quantum efficiency of photoelectric conversion.

The CdS/CIGS solar cell is generally treated as an abrupt asymmetric p-n heterostructure, in which the SCR (depletion layer) is practically located in the p-CIGS and the photoelectric conversion takes place almost in this layer (see [8] and references therein). The potential and field distributions in abrupt asymmetric p-n junction are practically the same as in a Schottky diode, therefore, further consideration of the processes in CdS/CIGS solar cells can be studied on the basis of the concepts developed for Schottky diodes.

The exact expression for the photovoltaic quantum efficiency of a p-type semiconductor Schottky photodiode obtained from the continuity equation taking into account the recombination at the front surface has the form [21]:

$$\eta(\alpha) = \frac{1 + S_f / D_p \exp(-W^2 / W_o^2)\ \ [A(\alpha) - D_p \Delta n / \Phi]}{1 + (S_f / D_p)\ \exp(-W^2 / W_o^2)\ B} - \frac{\exp(-\alpha W)}{1 + \alpha L_n} - \frac{D_n}{L_n}\frac{\Delta n}{\Phi}, \tag{20}$$

http://dx.doi.org/10.5772/59363

where α is the absorption coefficient, S_f is the recombination velocity at the front surface, D_n and D_p are the diffusion coefficients of electrons and holes, respectively, L_n is the diffusion length of electrons, Δn is the excess concentration of electrons at $x=W$, which is equal to

$$\Delta n = \Phi \frac{F_5}{D_p}. \tag{21}$$

In Eqs. (20) and (21)

$$F_5 = \frac{F_4 - F_3 \exp(-\alpha W)/(1+\alpha L_n)}{1 + F_3 / L_n}, \tag{22}$$

$$F_3 = \int_o^W \exp\{-[(x-W)/W_o]^2\}dx, \tag{23}$$

$$F_4 = \int_o^W \exp\{-\alpha x - [(x-W)/W_o]^2\}dx, \tag{24}$$

and the following notations are used:

$$W_o = \sqrt{\frac{2\varepsilon\varepsilon_o kT}{q^2(N_a - N_d)}}, \tag{25}$$

$$F_4 = \int_o^W \exp\{-\alpha x + [(x-W)/W_o]^2\}dx, \tag{26}$$

$$B = \int_0^W \exp[(x-W)/W_o]^2 dx, \tag{27}$$

where the $W_o / 2^{1/2}$ value is the Debye length.

In a CIS or CIGS with both acceptor and donor impurities, the SCR width W given in the above equations is determined by the expression [22]:

$$W = \sqrt{\frac{2\varepsilon\varepsilon_o(\varphi_{bi} - qV)}{q^2(N_a - N_d)}}, \tag{28}$$

where ε is the relative permittivity of CIGS (ε=13.6), ε_o is the permittivity of vacuum, and N_a – N_d is the concentration of uncompensated acceptors (not the free hole density).

For the convenience in analyzing the dependence of η on the parameters of the diode structure, the expression (20) can be simplified.

In a solar cell, CIS or CIGS, with the barrier height from the semiconductor side φ_{bi} is of the order of 1 eV and the width of the SCR is about 1 μm, i.e., the electric field is close to 10^4 V/cm. At the boundary between the depletion layer and the neutral region (x=W), the photogenerated electrons are pulled into the SCR by strong electric field, and without causing error, one can assume that Δn=0 and disregard the terms containing Δn in Eq. (20) [21].

The integrand $f(x)$ in Eq. (24) decreases exponentially as x increases. Therefore, we can replace the integration by the multiplication of the maximum value of the function $\exp(W/W_o)^2$ by its "half-width", which is determined by the value of x_2 at the point where the value of $f(x)$ is smaller than the peak value by a factor e=2.71.

Thus, we can find the value of x that satisfies this condition from the equality:

$$\exp\{-\alpha x_2 + [(x_2 - W)/W_o]^2\} = \exp(W/W_o)^2 e^{-1} = \exp\left[(W/W_o)^2 - 1\right], \tag{29}$$

which is reduced to the quadratic equation

$$x_2^{\,2} - (\alpha W_o^2 + 2W)x_2 + W_o^2 = 0 \tag{30}$$

with the solution

$$x_2 = \frac{\alpha W_o^2 + 2W}{2}[1 - \sqrt{1 - 4W_o^2/(\alpha W_o^2 + 2W)^2}]. \tag{31}$$

Since the second term under the square root is much less than unity, $\sqrt{1-x} \approx 1 - x/2$,

$$x_2 \approx [\alpha + 2W/W_o^2]^{-1} = [\alpha + 2(\varphi_{bi} - qV)/2kTW]^{-1}. \tag{32}$$

Similarly, by replacing the integration in Eq. (23), we can obtain the expression for x_2 in the form

$$x_2 \approx [2(\varphi_{bi} - qV)/2kTW]^{-1}. \tag{33}$$

http://dx.doi.org/10.5772/59363

So, considering all the simplifications made for the photoelectric quantum yield it is possible to substitute Eq. (20) with the following expression:

$$\eta_{\text{int}} = \frac{1 + S_f / D_p \ [\alpha + (2/W)(\varphi_{bi} - qV)/kT]^{-1}}{1 + S_f / D_p \ [(2/W)(\varphi_{bi} - qV)/kT]^{-1}} - \frac{\exp(-\alpha W)}{1 + \alpha L_n}. \tag{34}$$

As an example comparison of the curves $\eta_{\text{int}}(\lambda)$, calculated using the exact Eq. (20) and Eq. (34) is shown in Fig. 10 in the case of the spectrum of $CuInSe_2$ solar cell.

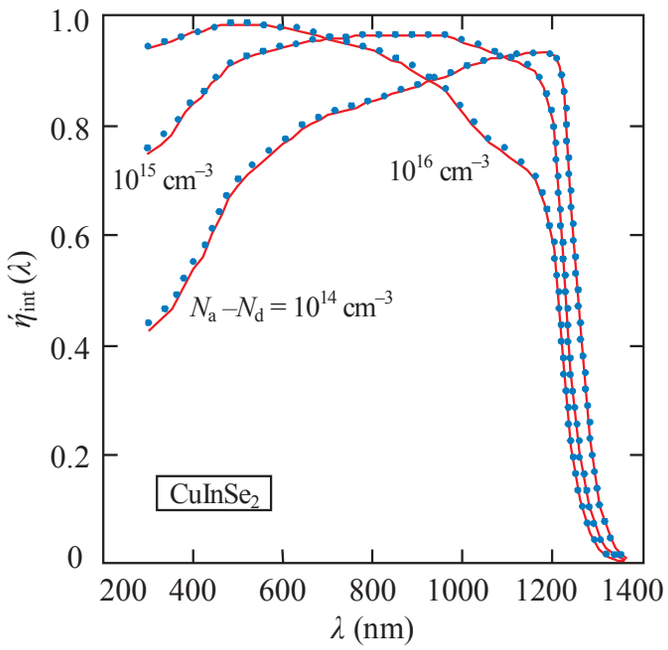

Figure 10. The quantum efficiency spectra of $CuInSe_2$ solar cell calculated by the exact formula (20) (solid line) and the simplified formula (34) (dotted line).

In the calculations we used the absorption curve $\alpha(\lambda)$ and typical parameters for this cell (see Table 2): barrier height φ_{bi}, the diffusion coefficients of electrons D_n and holes D_p, their mobility μ_n and μ_p, the electron lifetime τ_n ($L_n=(\tau_n D_n)^{1/2}$), the surface recombination velocity S_f, and the concentration of uncompensated acceptors $N_a - N_d$ which varied in the range 10^{14}-10^{16} cm^{-3}. As seen, variation of $N_a - N_d$ modifies the shape of the $\eta_{\text{int}}(\lambda)$ spectra, but in all cases the curves calculated by Eqs. (20) and (34) are very close, i.e., Eq. (34) represents well the results of the exact calculation.

It should be bear in mind that Eq. (34) takes into consideration both the drift and diffusion components of the quantum efficiency but does not take into account recombination at the back surface of the absorber layer [21] which can result in significant losses in the case of a thin-film solar cell. In the case of CdS/CdTe cell, for example, it is possible to neglect the recombination at the back surface if the thickness of the absorber exceeds 4–5 μm. However,

solar cells with thinner layers are also of considerable interest. In this case, Eq. (34) is not valid, and the drift and diffusion components of the quantum efficiency should be separated.

To find an expression for the drift component of the photoelectric quantum yield one can use Eq. (34). Indeed, the absence of recombination at the front surface (S_f=0) transforms this equation into the known Gartner formula:

$$\eta = 1 - \frac{\exp(-\alpha W)}{1+\alpha L_n}. \tag{35}$$

The above equation also ignores recombination at the back surface of the absorbed layer. Eq. (34) does not take into account recombination inside the SCR, therefore, subtracting the absorptive capacity of the SCR layer 1 – exp(–αW) from the right side of Eq. (34), we obtain the expression for the diffusion component of the quantum yield for a thick solar cell exp(–αW) $\alpha L_n/(1+\alpha L_n)$ which ignores recombination at the back surface. Upon eliminating the diffusion component from the right side of Eg. (34) we come to the expression for the drift component of the quantum efficiency which take into account the surface recombination at the front surface of the absorber:

$$\eta_{\text{drift}} = \frac{1+S_f/D_p\left(\alpha+2(\varphi_{bi}-qV)/WkT\right)^{-1}}{1+S_f/D_p\ \left(2(\eta_{ext}\varphi_{bi}-qV)/WkT\right)^{-1}} - \exp(-\alpha W). \tag{36}$$

For the diffusion component of the photoelectric quantum efficiency taking into account surface recombination at the back surface of the absorber layer, one can use the exact expression obtained for the p-layer in a solar cell with p-n junction [22]:

$$\eta_{\text{dif}} = \frac{\alpha L_n}{\alpha^2 L_n^2 - 1}\exp(-\alpha W)\times \\ \times\left\{\alpha L_n - \frac{S_b L_n/D_n\left[\cosh[(d-W)/L_n] - \exp\left(-\alpha(d-W)\right)\right] + \sinh[(d-W)/L_n] + \alpha L_n \exp(-\alpha(d-W))}{(S_b L_n/D_n)\sinh[(d-W)/L_n] + \cosh[(d-W)/L_n]}\right\}, \tag{37}$$

where d is the thickness of the absorber layer and S_b is the recombination velocity at the back surface.

The internal quantum efficiency of photoelectric conversion in the absorber layer is the sum of the two components:

$$\eta_{\text{int}} = \eta_{\text{drift}} + \eta_{\text{dif}}, \tag{38}$$

whereas the external quantum efficiency can be written in the form

http://dx.doi.org/10.5772/59363

$$\eta_{ext} = T(\lambda)(\eta_{drift} + \eta_{dif}), \tag{39}$$

where $T(\lambda)$, as mentioned previously, is the optical transmission of the ZnO and CdS layers determined by Eq. (8).

Fig. 11 shows a comparison of the measured quantum efficiency spectra of $CuInSe_2$, $CuIn_{0.69}Ga_{0.31}Se_2$ and $CuIn_{0.34}Ga_{0.66}Se_2$ solar cells taken from [8] with the results of calculations using Eq. (39). Note that the data on the extinction coefficients (and hence the absorption coefficient α) used in this and following calculations were measured for E_g=1.02, 1.16 eV and E_g=1.38 eV [12] rather than 1.04, 1.14 and 1.36 eV, respectively [8] that explains the slight blue shift (10-20 nm) in the calculated long-wavelength edge of the spectra in Fig. 11.

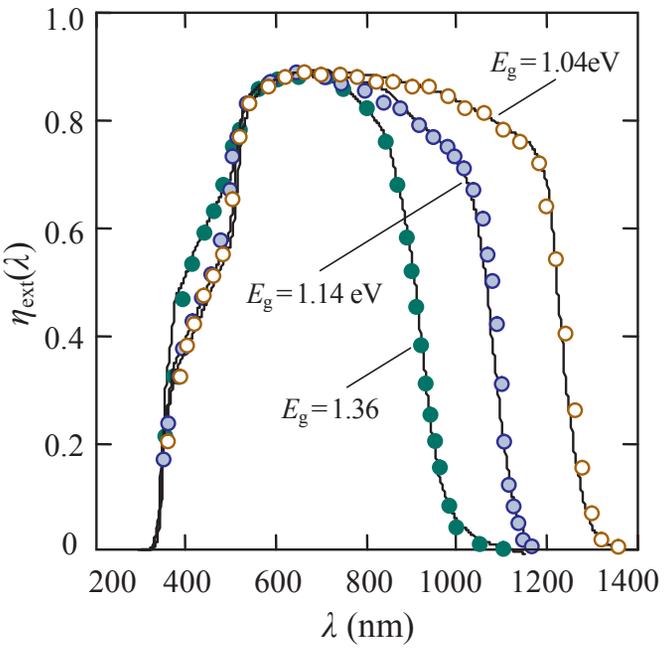

Figure 11. Comparison of the measured (circles) [8] and calculated (solid lines) quantum efficiency spectra of $CuInSe_2$ (E_g=1.04 eV), $CuIn_{0.76}Ga_{0.24}Se_2$ (E_g=1.14 eV) and $CuIn_{0.39}Ga_{0.61}Se_2$ (E_g=1.36 eV) solar cells.

According to the data in the above reference [8], in the calculations, the thicknesses of the CIGS, ZnO, CdS and MgF_2 layers were assumed to be 2000, 300, 20–50 and 100 nm, respectively. The parameters of the absorber layer were varied within the limits reported in the literature. It should be noted that for polycrystalline CIGS, there is a large spread in mobility values of electrons and holes. At room temperature, the values of the hole mobility are most often indicated in the range from 1–5 to 30–50 $cm^2/(Vs)$ and from 1 to 100 $cm^2/(Vs)$ for the electron mobility [23–25]. Unlike this, it was found in [26] that the electron and hole mobilities in $Cu(In,Ga)Se_2$ are much lower than 1 $cm^2/(Vs)$. As mentioned in Section 2, we believe that such low mobilities refer to the charge transport in the sub-band joined with the conduction band (valence band) due to high doping or/and disorder in the crystal lattice. In contrast, electrons and holes arising as a result of absorption of photons with the energy $h\nu \geq E_g$ and involving in

the photocurrent formation are moving in the conduction and valence band, where their mobilities are much higher.

The lifetime of minority carriers (electrons), determining their diffusion length $L_n=(\tau_n D_n)^{1/2}$ has also a significant impact on the efficiency of solar cells. As reported back in 1996 [27], the lifetimes of electrons in $CuInSe_2$ are in the range of tens of picoseconds to a few nanoseconds, which was subsequently confirmed in [23, 28]. Lifetime of minority carriers affects the diffusion component of photocurrent and therefore reveals itself in the long-wavelength range ($\lambda >$ 600-700 nm) of the spectrum.

Yet another important parameter determining the quantum efficiency spectra of solar cells is the concentration of uncompensated acceptors $N_a - N_d$ in the absorber, which according to Eq. (28) determines the width of the SCR. At high $N_a - N_d$, the width of the SCR amounts to a small portion of the absorber thickness. With decreasing $N_a - N_d$, the efficiency of cell increases since more and more part of the radiation is absorbed in the SCR, where the photogenerated electrons and holes move apart in the opposite directions by the electric field and reach the contacts without recombination. However, an increase of the quantum efficiency due to expansion of the SCR occurs only to a certain extent, because with increasing W, the electric field in the SCR is weakened and, therefore, recombination at the front surface of the absorber layer is intensified. As a result, the quantum efficiency in the low wavelength region reduces.

The velocity of recombination at the front surface S_f affects the efficiency in a wide range of wavelengths (excluding the long wavelength part) and more stronger in a wider SCR.

Our calculations in section 4.3 show that recombination at the rear surface of 2 μm thick absorber layers of $CuInSe_2$, $CuIn_{0.76}Ga_{0.24}Se_2$ and $CuIn_{0.39}Ga_{0.61}Se_2$ manifests itself very weakly and only for long lifetimes of electrons.

It follows that the main parameters of the absorber layer affect the QE spectrum of the solar cell *differently* [29]. This facilitates the choice of the parameter values for better agreement between the calculated and experimental data and virtually eliminates getting the same spectral curve for different combinations of parameters. The data of calculations presented in Fig. 12 confirm the above statement showing how the spectrum of $CdS/CuInSe_2$ solar cell is modified when one of the parameters is varied.

As can be seen, a deviation upward or downward from the optimum value of the minority carrier lifetime (τ_n=2 ns) substantially affect the spectral distribution of the quantum efficiency only at wavelengths longer than ~ 700 nm. In contrast, the deviation of the recombination velocity at the front surface of the $Cu(In,Ga)Se_2$ layer from the value $S_f=2\times10^5$ cm/s results in significant changes in the short wavelength region (shorter than ~ 800 nm). Judging the curves in Fig. 12b, it might give the impression that the recombination at the front surface has more or less the same effect on the quantum efficiency over the entire spectrum, and it can induce doubt in the correctness of the physical model used. However, this is not so, a simple calculation shows that for $S_f=10^7$ cm/s in the spectral range 600-800 nm, surface recombination reduces the quantum efficiency only by 2-4% but as high as ~ 22% in the range 350-400 nm.

The concentration of uncompensated acceptors $N_a - N_d$ impacts the entire spectrum, and is more appreciable. Moreover, when concentration of $N_a - N_d$ is deviated by an order from the

http://dx.doi.org/10.5772/59363

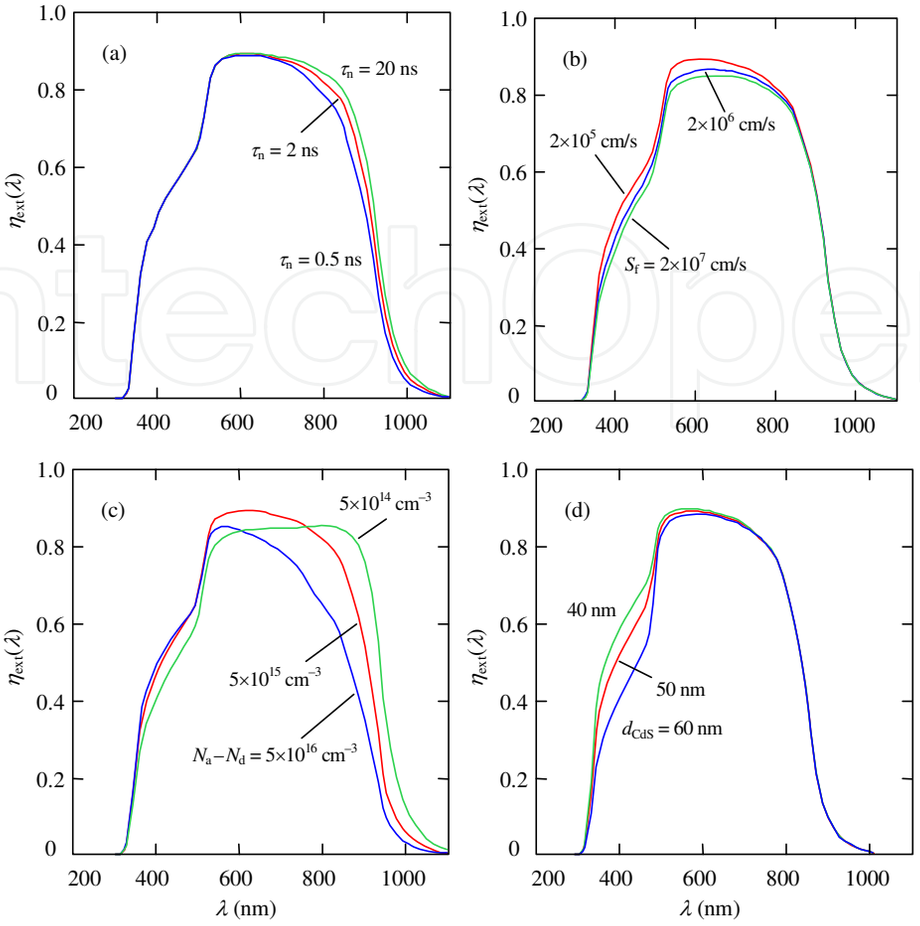

Figure 12. Effect of the electron lifetime τ_n (a), the surface recombination velocity S_f (b), the concentration of uncompensated acceptors $N_a - N_d$ (c) and the thickness of the CdS film (d) on the spectral distribution of the quantum efficiency of $CuInSe_2$ solar cell.

optimum value 5×10^{15} cm^{-3}, qualitative changes are observed in the spectrum, notably in the range λ=550-850 nm, increasing the efficiency with wavelength is replaced by its decay when $N_a - N_d$ is increased.

Finally, the variation of the CdS layer thickness manifests itself only in the range of the fundamental absorption of this semiconductor, i.e., when $\lambda < 500$ nm.

Parameters giving best match for the spectral distribution of calculated and experimental QE of the studied cells are summarized in Table 2. Notice that in the investigated solar cells, the SCR width (0.4–0.6 μm) amounts to a small part of the thickness of the absorber layer and the recombination velocity S_f is equal to $\sim 10^5$ cm/s, i.e., S_f is low as compared to thin-film CdS/CdTe heterostructure. This is explained by the known peculiarity of CdS/CIGS heterojunction.

Back in the late 1980s, it was shown that the CIGS solar cells are insensitive to defects caused by a lattice mismatch or impurities at the CdS/CIGS interface. In fact, the lattice mismatch is rather small for CdS and $CuInSe_2$ ($\sim$ 1%) and weakly increases with the Ga content. In addition, the deposition of CdS on the treated and cleaned surface of the CIGS layer is characterized by

pseudo-epitaxial growth, and the intermixing of the heterojunction constituents is observed even at relatively low-temperature processes [30, 31].

Solar cell	E_g (eV)	φ_{bi} (eV)	τ_n (ns)	$N_a - N_d$ (cm^{-3})	S_f (cm/s)	d_{CdS} (nm)
$CuInSe_2$	1.04	0.60	5	2×10^{15}	1×10^{5}	45
$CuIn_{0.3}Ga_{0.7}Se$	1.14	0.75	20	9×10^{15}	5×10^{5}	50
$CuIn_{0.67}Ga_{0.3}Se$	1.36	0.95	2	5×10^{15}	2×10^{5}	40

Table 2. Parameters of $CuInSe_2$, $CuIn_{0.76}Ga_{0.24}Se_2$ and $CuIn_{0.39}Ga_{0.61}Se_2$ solar cells giving better match between measured and calculated data

A comparison of measured and calculated results presented in Fig. 11 shows that the theoretical model describes in detail the spectral distribution of the quantum efficiency of CIGS solar cells, which is important for further analysis of recombination losses. But the question arises, how this model can be applicable in polycrystalline material, with its inhomogeneity, recombination at the grain boundaries, etc. A possible explanation for the applicability of the model in question to efficient solar cells based on polycrystalline CIGS is that during the growth of the absorber layer and post-growth processing, recrystallization leading to grain growth and their coalescence occur. Also no less important is the fact that a structure in the form of ordered columns oriented perpendicular to the electrodes is created in the CIGS layer (see reviews [32] and references therein). One can assume that in a layer of columnar structure, collection of photogenerated charge occurs without crossing the grain boundaries. In addition, the scattering and recombination on the lateral surfaces of the columns also have no significant effect due to the strong electric field in the barrier region.

Indeed, the width of the SCR in the studied solar cell is about 0.5 μm, and the electric field at a barrier height φ_{bi} of about 1 eV is higher than 10^4 V/cm. Under such conditions, the drift length of charge carriers with the mobility of 20-30 $cm^2/(Vs)$, and lifetimes 10^{-9} s is several microns which is significantly greater than the width of SCR and makes recombination improbable. Outside the SCR, where the diffusion component of photocurrent is formed, the electric field does not exist, but due to the high absorption capacity of CIGS the vast majority of solar radiation is absorbed in the SCR. This is illustrated in Fig. 13 with the example of $CuIn_{0.39}Ga_{0.61}Se_2$ (E_g=1.36 eV) solar cell, where the quantum efficiency spectra along with the drift and diffusion components are shown. As expected, the diffusion component falls mostly on the long-wavelength part of spectra (λ longer than ~ 600 nm) and its contribution to the quantum efficiency is quite insignificant.

Calculation given by Eq. (39) shows that for the parameters listed in Table 2, the contributions of the diffusion component in the photocurrent of $CuInSe_2$, $CuIn_{0.76}Ga_{0.24}Se_2$ and $CuIn_{0.39}Ga_{0.61}Se$ solar cells is about 2, 4 and 8%, which are far inferior to the drift component. This significantly weakens the role of recombination at the grain boundaries.

http://dx.doi.org/10.5772/59363

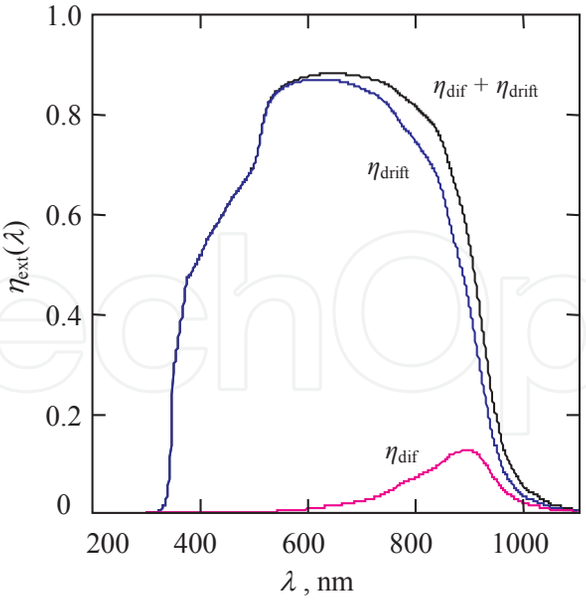

Figure 13. Drift and diffusion components of the quantum efficiency of $CuIn_{0.39}Ga_{0.61}Se_2$ solar cell and their sum.

4.1. Recombination losses at the absorber front surface

To determine the recombination losses, we will calculate the photocurrent density by varying the parameters of solar cells such as the recombination velocity at the absorber surface, concentration of uncompensated acceptors and carrier lifetimes in the material, as well as the thickness of the absorber. Photocurrent density will be calculated by Eq. (19) using for $T(\lambda)$ Eq. (39).

Until now, the internal quantum efficiency was calculated under zero bias, since it was necessary for comparison with the spectra measured at V=0. However, recombination losses should be calculated in the operating mode of the solar cell, i.e., at the voltage V_m, which maximizes the generated electrical power. As will be shown in Section 5.3, these voltages V_m are 0.36, 0.46 and 0.63 V for $CuInSe_2$, $CuIn_{0.76}Ga_{0.24}Se_2$ and $CuIn_{0.39}Ga_{0.61}Se_2$ solar cells, respectively.

Consider how the photocurrent density J varies depending on the concentration of uncompensated acceptors at different recombination velocities at the front surface of the CIGS absorber. Note that according to Eq. (36), the recombination does not depend on the carrier lifetime in this case. Fig. 14 shows for $CuIn_{0.39}Ga_{0.61}Se_2$ solar cell the dependences of J on $N_a - N_d$ in the range 5×10^{14}–10^{18} cm^{-3} and S_f in the range 10^4–10^7 cm/s and also at S_f=0. The lower range of $N_a - N_d$ is limited to 5×10^{14} cm^{-3}, because at this values the width of the SCR becomes greater than the thickness of the absorber layer d=2 μm.

As seen in Fig. 14a, if the concentration of uncompensated acceptors exceeds 10^{17} cm^{-3}, surface recombination does not reveals itself, but at lowering the $N_a - N_d$, the decrease in J becomes appreciable. At S_f=10^4 cm/s, recombination practically does not reduce the current and slightly lowers it at the real values of $N_a - N_d$=5×10^{15} cm^{-3} and S_f=2×10^5 cm/s for this solar cell. As our calculations show in Fig. 14b, for $CuIn_{0.39}Ga_{0.61}Se$ solar cell, surface recombination reduces J by

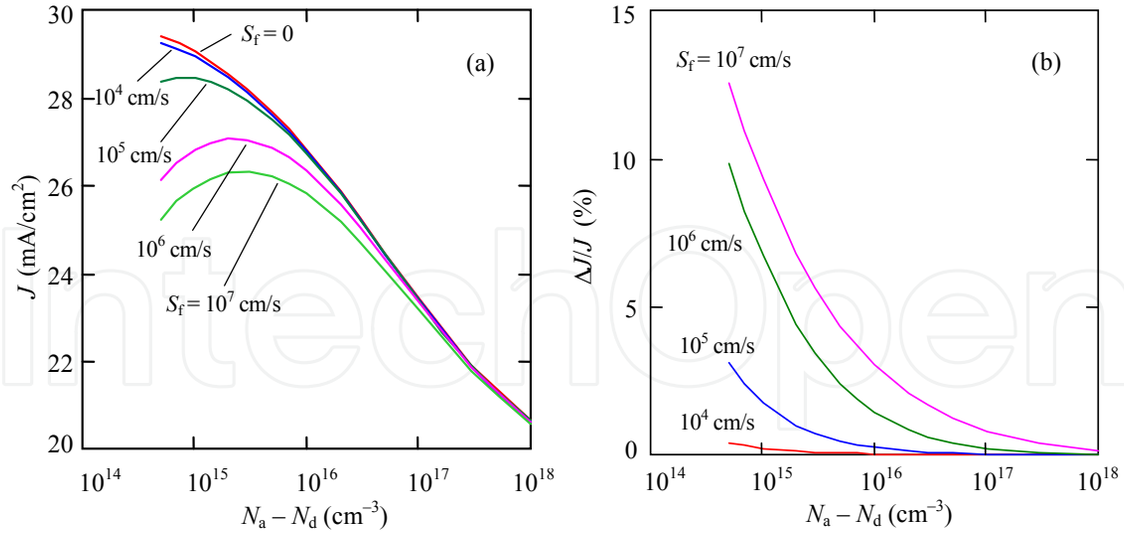

Figure 14. (a) Photocurrent density J as a function of the concentration of uncompensated acceptors $N_a - N_d$ at different recombination velocities S_f at the front surface of the CIGS absorber in $CuIn_{0.39}Ga_{0.61}Se$ solar cell. (b) Reduction in the photocurrent density, expressed as in percentage.

1.8% for $N_a - N_d = 5 \times 10^{15}$ cm^{-3}. Similar calculations carried out for $CuInSe_2$ and $CuIn_{0.76}Ga_{0.24}Se_2$ solar cells show that recombination losses for them are equal to 2.1% and 1.9%, respectively. Relatively small recombination losses are explained by the above mentioned fact that the CIGS solar cells are insensitive to defects at the CdS/CIGS interface due to pseudo-epitaxial growth of the CIGS and the intermixing of the heterojunction constituents.

4.2. Recombination losses in the SCR

Recombination of photogenerated charge carriers in the SCR can be taken into account, using the well-known Hecht equation [33]:

$$\eta_H(x) = \frac{\lambda_n}{W}\left[1 - \exp\left(-\frac{x}{\lambda_n}\right)\right] + \frac{\lambda_p}{W}\left[1 - \exp\left(-\frac{W - x}{\lambda_p}\right)\right], \tag{40}$$

where x is the coordinate (x is measured from the CdS/CIGS interface), λ_n and λ_p are the drift lengths of electrons and holes in the SCR:

$$\lambda_n = \mu_n F \tau_{no}, \tag{41}$$

$$\lambda_p = \mu_p F \tau_{po}, \tag{42}$$

F is the electric field strength; τ_{no} and τ_{po} are the lifetimes of electrons and holes in the SCR, respectively, which we will accept to be equal to τ_n assuming that the CIGS absorber is a highly doped semiconductor.

http://dx.doi.org/10.5772/59363

In CdS/CIGS heterostructure, the electric field is not uniform, but the problem of the nonuniformity is simplified, since the field strength F decreases in a Schottky diode linearly with the x coordinate. In this case, F in the expressions (41) and (42) can be replaced by the average values of F in the sections $(0,x)$ and (x,W) for electrons and holes, respectively, i.e.,

$$F(0,x) = \frac{\varphi_{bi} - qV}{qW}\left(2 - \frac{x}{W}\right), \tag{43}$$

$$F(x,W) = \frac{\varphi_{bi} - qV}{qW}\left(1 - \frac{x}{W}\right). \tag{44}$$

Evidently, charge collection efficiency in the dx interval of the SCR is $\eta_H \alpha \exp(-\alpha x)dx$ and then the charge-collection efficiency for the wavelength λ_i is determined by expression:

$$\eta_H(\lambda_i) = \int_0^W \eta_H(x)\alpha_i \exp(-\alpha_i \cdot x)dx. \tag{45}$$

Fig. 15 shows the photocurrent density J in $CuIn_{0.39}Ga_{0.61}Se_2$ as a function of the concentration of uncompensated acceptors $N_a - N_d$ at different carrier lifetimes given by the equation:

$$J = q\sum_i \frac{\Phi_i(\lambda_i)}{h\upsilon_i} T(\lambda_i)\eta_H(\lambda_i)\Delta\lambda_i. \tag{46}$$

As can be seen in Fig. 15a, when $N_a - N_d > 3\times10^{16}$ cm^{-3} ($W < 0.2$-0.3 μm), the curves calculated for different lifetimes of charge carriers $\tau_n=\tau_{no}=\tau_{po}$ coincide, but as the SCR width increases, the curves diverge and become more pronounced when τ_n is less. The reduction of J due to recombination can be found by subtracting the current at a given τ_n from the value of current j_o when recombination does not occur. The latter is possible for a sufficiently large lifetime of charge carriers. A simple calculation shows that when $\tau_n > 500$-600 ns, the current becomes independent of τ_n, therefore the values of j_o at different $N_a - N_d$ were found for τ_n=1000 ns (the curve j_o vs. $N_a - N_d$ is also shown in Fig. 15a).

Fig. 15b shows the reduction in J due to recombination in the SCR and its dependence on the $N_a - N_d$ and τ_n. As seen, when $N_a - N_d < 10^{16}$ cm^{-3} ($W > 1$ μm), the recombination losses increase rapidly up to 60% with decreasing $N_a - N_d$ and τ_n. The data presented in this figure allow determining the recombination losses for any values of $N_a - N_d$ and τ_n. For the real carrier lifetime of 2 ns and $N_a - N_d$=5×10^{15} cm^{-3}, which are characteristic of $CuIn_{0.39}Ga_{0.61}Se$ solar cell, the recombination losses amount to 1.0%, whereas for $CuIn_{0.76}Ga_{0.24}Se_2$ solar cell the losses is

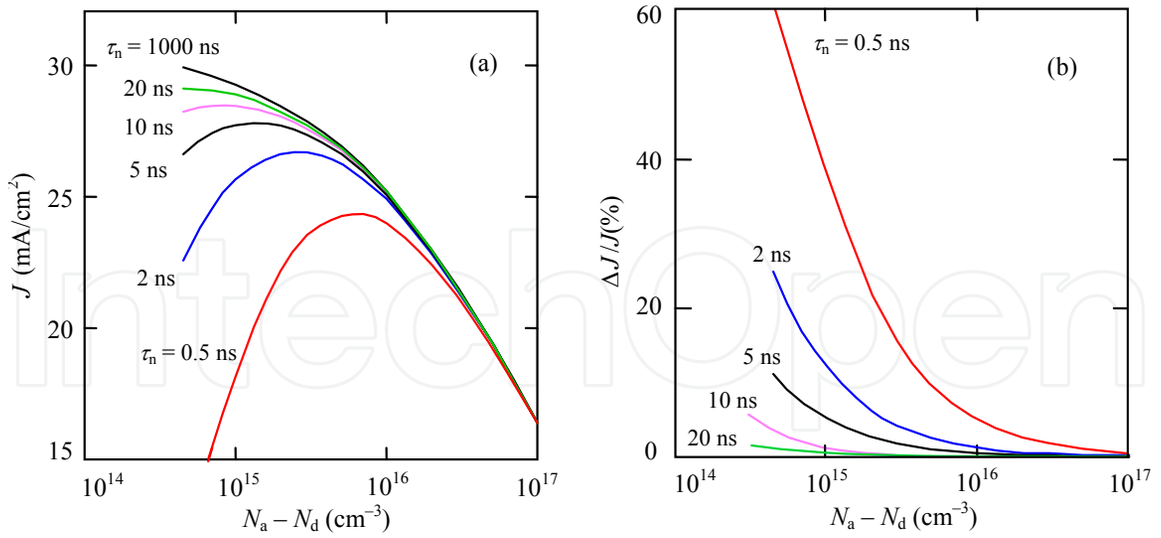

Figure 15. (a) Photocurrent density J as a function of the concentration of uncompensated acceptors $N_a - N_d$ for different carrier lifetimes τ_n in the $CuIn_{0.39}Ga_{0.61}Se_2$ absorber. (b) Reduction of the photocurrent density expressed in percentage.

only 0.1% because of higher values τ_n=20 ns and $N_a - N_d$=9×10^{15} cm^{-3}. For $CuInSe_2$ solar cell, the recombination losses due to recombination in the SCR amount to 0.7%.

4.3. Recombination losses at back surface and neutral part of absorber

Useful information about the effect of recombination at the back surface of the solar cell and the neutral part of the absorber on the photocurrent J can be obtained by studying the dependence of J on the absorber thickness d. If d is large, the effect of recombination at the back surface is imperceptible, but when the rear surface is close to the SCR by a distance comparable to the diffusion length of electrons, the role of recombination increases. This leads also to a decrease in the diffusion component of the photocurrent.

Subtracting the currents calculated for the recombination velocity S_b=10^7 cm/s and S_b=0, one can obtain the change of J due to recombination at the back surface. Obviously, for longer minority-carrier lifetime, recombination at the back surface of the absorber is intensified and manifests itself also at larger absorber thickness.

Fig. 16a shows the dependences of photocurrent J on the thickness d of the $CuIn_{0.39}Ga_{0.61}Se_2$ absorber calculated for S_b=10^7 cm/s and S_b=0 and at different lifetimes of electrons. As it is shown by dashed lines, when the $CuIn_{0.39}Ga_{0.61}Se_2$ layer becomes thinner, the photocurrent for S_b=0 first slightly grows and then rapidly decreases. The observed current growth can be explained by the fact that the diffusion component of the photocurrent is determined by the derivative of the excess concentration of photogenerated electrons $\Delta n/dx$ [22]. The derivative may be larger than that in the absence of recombination at the surface, but when d approaches the cross section x=W, the diffusion component eventually decreases due to reduced the Δn absolute value and next Δn=0 when x=W. This also explains why the dependence of ΔJ / J on d shown in Fig. 16b is described by a curve with a maximum.

http://dx.doi.org/10.5772/59363

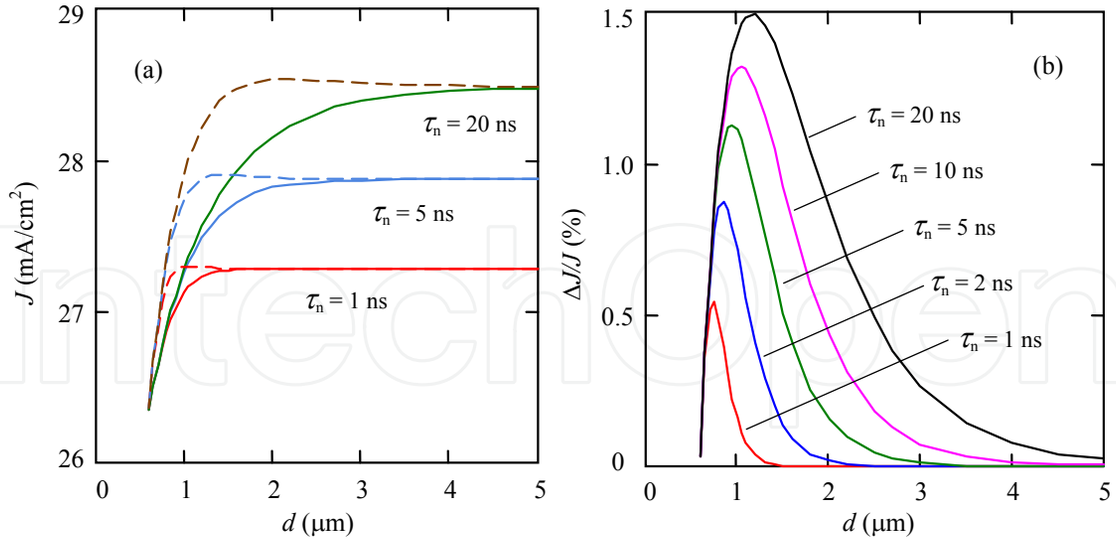

Figure 16. (a) Dependences of the photocurrent density on thickness of the $CuIn_{0.39}Ga_{0.61}Se_2$ layer calculated for different electron lifetimes with and without taking into account recombination at the back surface of the absorber (solid and dashed lines, respectively), (b) Decrease in photocurrent density due to recombination at the back surface calculated for different electron lifetimes.

As can be seen from Fig. 16b, the decrease in photocurrent does not exceed 1.5% even with lifetimes of electrons 20 ns. With such low recombination losses, the creation of a heavily doped layer adjacent to the back contact as it is proposed in CdS/CdTe solar cells [7] or to form a bandgap gradient outside the SCR in the CIGS absorber [8] to reduce the negative impact of recombination at the rear surface of the absorber seems to be unreasonable. As previously mentioned, a very small fraction of carriers taking part in the photocurrent formation (2–8%) falls on the neutral part of the studied CIGS solar cells that also should be borne in mind.

Of course, recombination of photogenerated carriers happens not only at the back surface of the absorber, but also in whole neutral part (outside the SCR). The losses due to such recombination can be found as the difference between photocurrent at: (i) real electron lifetime and recombination velocity at the rear surface and (ii) large value of the electron lifetime when recombination can be ignored (τ_n=1000 ns) and S_b=0. As the calculations show, such losses are 2.5, 5.0 and 2.9% for $CuInSe_2$, $CuIn_{0.76}Ga_{0.24}Se_2$ and $CuIn_{0.39}Ga_{0.61}Se_2$ solar cells, respectively. It is necessary to emphasize that recombination in the neutral part of the absorber and at the rear surface are not additive. But the calculation results for the neutral part, for example, with and without recombination at the rear surface of the absorber differ slightly. Nevertheless the determination of the combined influence of recombination in the neutral part of the absorber and at its rear surface is more correct.

The calculated values of *all types of recombination losses* along with the corresponding decrease in the photocurrent J (given in brackets) are summarized in Table 3. Analysis of obtained results allows us to formulate some recommendations to improve the photoelectric conversion efficiency in the solar cells studied.

The total recombination losses in $CuInSe_2$, $CuIn_{0.76}Ga_{0.24}Se_2$ and $CuIn_{0.39}Ga_{0.61}Se_2$ solar cells amount to 5.4, 7.0 and 4.1%, respectively. It can be assumed that the charge collection efficiency of the photogenerated charge in the absorber is 94.6, 93.0 and 95.9%, respectively. Having these data, it is worth to analyze the possibility of reducing the recombination losses and improving the charge collection efficiency that we will make with an example of $CuIn_{0.76}Ga_{0.24}Se_2$ solar cell.

Origin of recombination losses	Losses in solar cell		
	$CuInSe_2$	**$CuIn_{0.76}Ga_{0.24}Se_2$**	**$CuIn_{0.39}Ga_{0.61}Se_2$**
Front surface	2.2% (0.9 mA/cm^2)	1.9% (0.7 mA/cm^2)	0.2% (< 0.1 mA/cm^2)
Space-charge region	0.7% (0.4 mA/cm^2)	0.1% (< 0.1 mA/cm^2)	1.0% (0.3 mA/cm^2)
Neutral part of absorber and back surface	2.5% (1.0 mA/cm^2)	5.0% (1.8 mA/cm^2)	2.9% (1.0 mA/cm^2)
Only back surface	0.2% (< 0.1 mA/cm^2)	1.0% (0.4 mA/cm^2)	0.1% (< 0.1 mA/cm^2)
Total recombination losses	5.4% (2.3 mA/cm^2)	7.0% (2.5 mA/cm^2)	4.1% (1.4 mA/cm^2)

Table 3. Recombination and the corresponding *J* losses in CIGS solar cells

According to Eq. (36), the recombination losses at the front surface can be lowered by increasing the hole diffusion coefficient $D_p=kT\mu_p/q$, i.e., increasing the mobility of holes μ_p. The results of calculation from Eq. (19) show that increasing the hole mobility from 30 to 300 cm^2/(Vs) (this is real according to the literature data) reduces such losses from 1.9 to 0.3%.

Significant improvement of the charge collection efficiency can be achieved by increasing the lifetime of electrons, which is equivalent to an increase of electron mobility since the diffusion length L_n is equal to $(\tau_n D_n)^{1/2}$. Increase in electron mobility also by an order of magnitude from 20 to 200 cm^2/(V s) leads to a reduction of the recombination losses in the neutral part of the absorber and at its rear surface from 5.0 to 1.1%.

The recombination losses in the SCR 0.1% at large electron and holes mobilities approach to zero since the drift lengths of carries are proportional to the their mobilities. Thus, due to a real increase of the mobility of electrons and holes by one order of magnitude the charge collection efficiency improves from 93.0 to 98.6%.

An even greater improvement of the charge collection efficiency can be achieved by extending the SCR, which leads to absorption of a greater part of the radiation in the SCR and hence the better collection of the photogenerated charge. However, one should keep in mind that when the electron lifetime and mobility increase, the diffusion length becomes longer than the absorber thickness. This weakens the desired effect and in fact the charge collection efficiency for d=2 μm is 96.2%.

There is also a positive impact for a higher carrier lifetime and expanded SCR since it leads to a decrease in the forward recombination current. Analyzing the electrical characteristics of the

http://dx.doi.org/10.5772/59363

solar cell, it is not difficult to show that this causes enhancing the open circuit voltage (see the next sections).

Some useful information can be obtained from the spectral distribution of the reflection, absorption and recombination losses. Fig. 17 shows the distribution of these losses over the whole spectrum for $CuIn_{0.76}Ga_{0.24}Se_2$ solar cell obtained from the results given above.

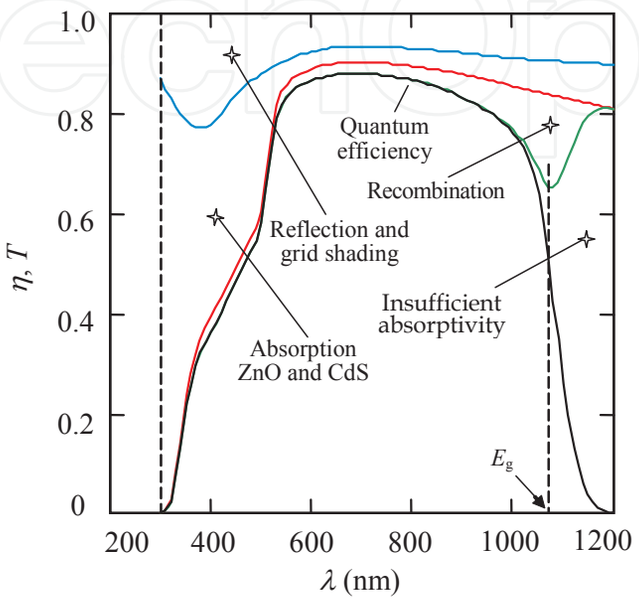

Figure 17. Illustration of spectral distribution of the reflection, absorption and recombination losses for $CuIn_{0.76}Ga_{0.24}Se_2$ solar cell (E_g=1.14 eV).

As clearly seen, the recombination losses are considerably less than those caused by reflection and absorption in the ZnO layer and especially in the CdS layer. The radiation in the range $h\nu < E_g$ gives a small contribution to the solar cell efficiency due to insufficient absorptivity of CIGS in this range, whereas at $h\nu > E_g$ slight decrease of the absorptivity compared to 100% takes place only when the photon energy is very close to E_g.

5. Electrical characteristics of CIGS solar cells

The electrical properties of CIGS solar cells are presented in many publications, but their *dark J–V* characteristics are practically absent and not discussed *analytically* in the literature with a few exceptions. This is despite the fact that the dark *J–V* relationship along with the quantum efficiency spectrum are the two key characteristics that determine substantially the performance of solar cells.

In this section we analyze the dark *J–V* characteristics of CIGS solar cells (x=0 – 0.61) extracted from the data under cell illumination reported in [8,34]. It is shown that the dark *J–V* curves are described by the theory of generation–recombination of charge carriers in the SCR

developed for the linearly graded silicon p-n junction in [19] and modified and adapted to a thin-film CdS/CdTe heterostructure taking into account peculiarities of the distribution of the electric potential and the concentrations of free electrons and holes in the SCR [29]. This is valid for CIGS solar cells taking into account the effect of the shunts at low forward voltages and the voltage drop across the series resistance at high forward currents. It is also shown that knowing the short–circuit current density (which can be obtained from spectra of the quantum efficiency and solar radiation), it is possible to calculate the *J*–*V* curves under illumination and find the open–circuit voltage, the fill factor and eventually the energy conversion efficiency. The electric losses caused by the presence of the shunts and series resistances of the bulk part of the CIGS absorber are also determined.

5.1. Experimental results and discussion

The *J*–*V* characteristics of CIGS solar cells having bandgaps of the absorber E_g=1.04, 1.14 and 1.36 eV under standard AM1.5 illumination taken from [8] are shown in Fig. 18a. The voltage dependences of the dark current derived from the difference between the short-circuit current density J_{sc} and the current density under illumination J_{IL} at each voltage are shown in Fig. 18b by solid (closed) circles, squares and triangles. At $V < 0.2$ V, the values of J_{IL} and J_{sc} are very close to each other, therefore the dark current cannot be determined with a proper accuracy.

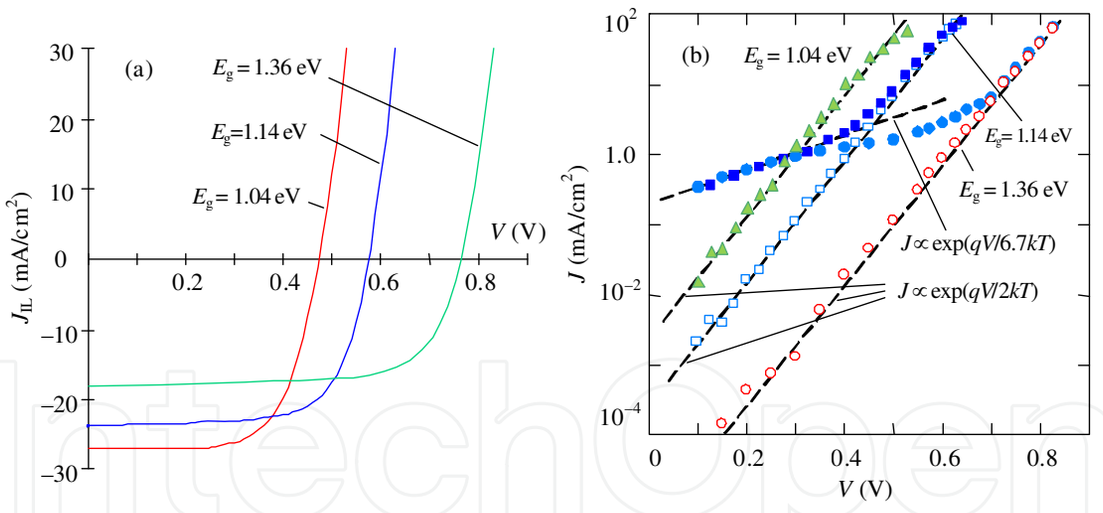

Figure 18. a) Voltage dependences of the current density in CIGS solar cells under illumination [8], (b) Dark currents (solid circles, squares, triangles) and currents obtained by subtracting the current through the shunt from the dark current in the absorber bandgaps 1.14 and 1.36 eV (open circles, squares).

As seen in Fig. 18b, the dark current in solar cell with the bandgap of the absorber 1.04 eV follows quite well the voltage dependence $J \propto \exp(qV/2kT)$ (dashed lines) in the range of almost four order of magnitude that confirms the recombination mechanism of charge transport suggested in [8, 34]. However, for the absorbers with the bandgap of 1.14 and 1.36 eV the *J*–*V* curves have a complicated form. As seen, the dependences $J \propto \exp(qV/2kT)$ are observed only at $V > 0.5$ and 0.7 V for the samples with E_g=1.14 (solid squares) and 1.36 eV (solid circles),

http://dx.doi.org/10.5772/59363

respectively. At lower voltage the *J–V* relationship deviates from such dependence for some reason. Note that, despite the significant difference of currents at higher voltages, the dark currents in these two cells at low voltages practically coincide and the *J–V* relationship can be interpolated by the expression $J \propto \exp(qV/AkT)$ with enormous large value of the ideality factor A=6.7.

Useful information about the electrical properties of the diode can be obtained from the analysis of the voltage dependence of the differential resistance $R_{dif}=dV/dI$ [22]. These dependences for three samples are shown in Fig. 19. It is known that the differential resistance of a semiconductor diode decreases exponentially with increasing forward voltage in a wide range including the lowest voltage as shown in Fig. 19 by dashed oblique straight lines. Such behavior of the differential resistance is observed only for $CuInSe_2$ diode (E_g=1.04 eV). For other two diodes, when a low forward voltage is applied, the dependence of R_{dif} on V deviates downward from the exponent and an invariance of R_{dif} takes place at the level of 0.3-0.4 Ω for diode area of 0.4 cm^2. It is quite realistic to assume that at low voltages, the current through the shunt rather than through the diode is dominant and only when bias is above 0.4 and 0.6 V respectively for devices with CIGS bandgaps E_g=1.14 and 1.36 eV, the diode currents are higher than that through the shunts (for CIS cell with bandgap E_g=1.04 the shunt is absent).

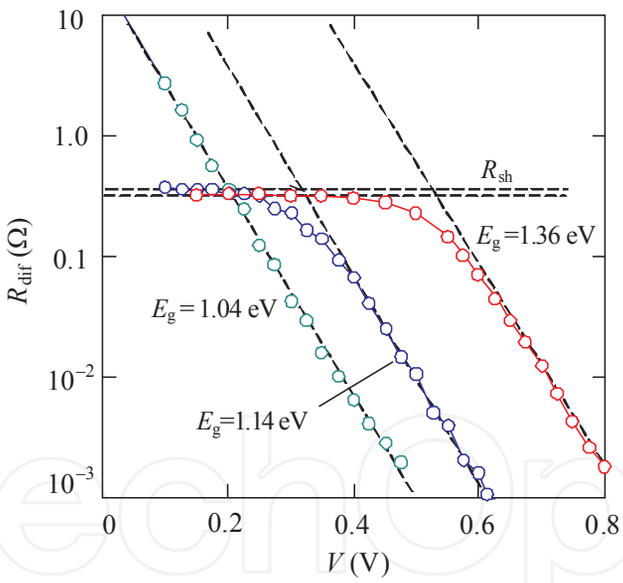

Figure 19. Voltage dependences of the differential resistance of the studied CIGS solar cells.

One can assume that shunting in the studied solar cells is caused by pin-holes and defects associated with a thin film of CdS (20–30 nm) used in the layered structure. In high efficiency CIGS solar cells, a thin intrinsic i-ZnO layer is applied which is capped by a thicker Al-doped ZnO layer. It is believed that the i-ZnO layer reduces the shunt paths by forming a thin high resistive transparent film (HRT), thin enough to promote tunneling, which is proven to enhance the device performance. However, ZnO is usually deposited by sputtering which is known as a damaging process [35]. Seemingly the damages at the CdS/CIGS interface pro-

duced by i-ZnO sputtering leads also to the occurrence of shunts. However, in the case of i-ZnO, the value of the shunt resistance is much larger compared to ZnO:Al due to high resistivity of i-ZnO and the shunting reveals itself only at relatively low voltages.

The voltage-independent differential resistance at $V < 0.2$ and 0.4 V for the two samples (Fig. 19) means that the shunt is a *linear* element of the electric circuit. Therefore, the effect of the shunt can be taken into account by subtracting the current through the shunt V/R_{sh} from the measured current J. The results of such manipulations for cells with the absorber bandgaps 1.14 and 1.36 eV are shown in Fig. 18b by open squares and circles, respectively, whereas the J–V curves without accounting for the shunt and series resistances are shown by solid circles and squares.

As seen in Fig. 18b, *qualitative* changes in the forward J–V characteristic of cells with the absorber bandgaps 1.14 and 1.36 eV occur after subtracting the current through the shunt resistance. In the range $V < 0.45$ V for the first cell (E_g=1.14 eV) and $V < 0.65$ V for the second cell (E_g=1.36 eV), the forward current rapidly decreases with decreasing the voltage by three and five orders of magnitude, respectively, continuing the same trend of the curves $J(V)$ as at the higher voltages. It is important to note that after subtracting the current through the shunt the current in the cells with the absorber bandgaps 1.14 and 1.36 eV as well as the measured current in a cell with the bandgap 1.04 eV ($CuInSe_2$) without shunting are proportional to $\exp(qV/AkT)$ at $A \approx 2$.

The obtained results can create the impression that the occurrence of shunt is due to the introduction of Ga into the $CuInSe_2$ crystal lattice in order to widen the semiconductor bandgap for increasing the efficiency of solar cells. However, some results reported in the literature indicate that the shunting in solar cells with wide bandgap can be avoided by modifying the fabrication technology, in particular by increasing the temperature of CIGS deposition and post-growth processing [36].

Soda-lime glass is a common substrate material used in CIGS solar cells due to its low cost and good thermal expansion match to $CuInSe_2$. In addition, the soda-lime glass supplies sodium to the growing CIGS layer by diffusion through the Mo back contact, leading to enhanced grain growth with a higher degree of preferred orientation.

It is known that the CIGS deposition requires a substrate temperature at least 350°C and efficient cells have been fabricated at the maximum temperature ~ 550°C, which the glass substrate can withstand without softening. In these temperature ranges, CIGS solar cells are typically made with low Ga content ($x \leq 0.3$) resulting in an absorber bandgap value of 1.1-1.2 eV. However as suggested by the theory, for optimum conversion efficiency it is desirable to open the bandgap up to E_g=1.4-1.5 eV.

It was shown in [36] that the growth and post-growth processing at temperature higher than 550°C leads to significant improvements of the performance of CIGS solar cells with bandgaps up to 1.4–1.5 eV. For this purpose, borosilicate glasses have been used in CIGS research even though it has non-optimum thermal coefficient of expansion and no sodium in it. Nevertheless the solar cells with a wide bandgap for CIGS absorber, fabricated on borosilicate glass at the substrate temperatures in the range of 600 to 650°C had a rather high efficiency.

http://dx.doi.org/10.5772/59363

In addition to improving efficiency, the shunting of heterostructure in the device fabricated at an elevated temperature can be eliminated. This is illustrated by Fig. 20 where the data obtained for solar cells with the absorber bandgap 1.5 eV fabricated using standard technology $T < 550$°C (sample #1) and at elevated temperature 600–650°C (sample #2) are shown by solid and open circles, respectively. The *J–V* curves for recombination current $J=J_o[\exp(qV/2kT) - 1]$ are also shown in Fig. 20a by solid lines *2* and *6*.

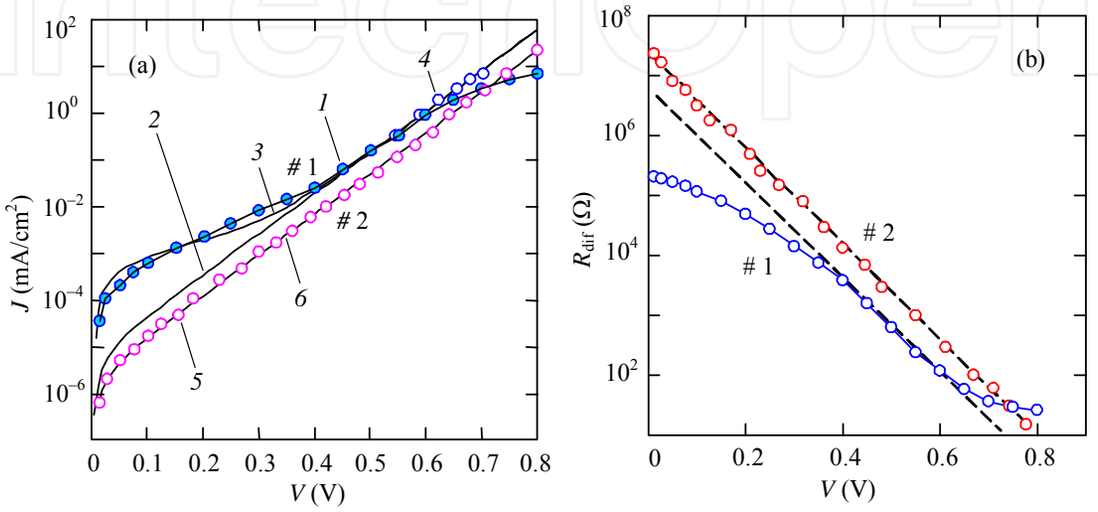

Figure 20. Voltage dependence of dark current density [36] (a) and differential resistance (b) of CIGS solar cells with absorber bandgap ~ 1.5 eV fabricated at standard temperature ≤ 550°C (sample #1) and elevated temperature 650°C (sample #2).

As can be seen in Fig. 20a, for solar cells fabricated using standard technology, the *J–V* relationship at $V < 0.4$ V deviates from the expression $J \propto [\exp(qV/2kT) - 1]$ (curve *#1*) that is caused by the effect of shunting. This observation is confirmed by the dependence of the differential resistance R_{dif} of this sample shown in Fig. 20b. As expected, the $R_{dif}(V)$ relationship deviates from the exponential decrease at low voltages in the range $V < 0.4$ V. However, the R_{dif} value does not become constant when the voltage approaches zero as it is observed in samples with the absorber bandgaps 1.14 and 1.36 eV in Fig. 19. Therefore, the shape of a measured curve cannot be accurately calculated by adding the current through the shunt V/R_{sh} to the recombination current. An approximate description of the measured curve is possible by taking the average value of the shunt resistance $R_{sh}=1.3\times10^5$ Ω. (line *3* in Fig. 20a).

The *J–V* relationship shown in Fig. 20a for sample #1 (solid circle) also deviates downward from the exponential increase at $V > 0.6$ V due to voltage drop across the series resistance R_s of the neutral part of the absorber layer. If this voltage drop is subtracted from *V*, a good agreement of theory with experiment can be achieved (curve *3* at $V > 0.6$ V).

As seen in Fig. 20a, the data obtained for solar cells fabricated at elevated temperature of 650°C is in good agreement with the expression $J=J_o[\exp(qV/2kT) - 1]$ over the whole voltage range. Thus, by growth and post-growth processing of the film at higher temperatures, CIGS solar

cells with wide bandgap for the absorber (up to 1.5 eV) can be fabricated without shunting at low voltages and the voltage drop across the series resistance at high currents.

5.2. Generation–recombination in space–charge region theory

As mentioned previously, the theory of generation–recombination of charge carriers in the space-charge region (SCR) was developed for the linearly graded silicon p-n junction by Sah et al. [19] and modified and adapted to a Schottky diode taking into account the distribution of the potential and free carrier concentrations in the SCR [37,38].

The generation–recombination rate through a single level trap for nonequilibrium but steady-state conditions in the cross section x of the SCR at voltage V is determined by the Shockley-Read-Hall statistics:

$$U(x,V) = \frac{n(x,V)p(x,V) - n_i^2}{\tau_{po}[n(x,V) + n_1] + \tau_{no}[p(x,V) + p_1]}, \tag{47}$$

where $n(x,V)$ and $p(x,V)$ are the carrier concentrations in the conduction and valence bands within the SCR, respectively; n_i is the intrinsic carrier concentration in the semiconductor; $\tau_{no}=1/\sigma_n \upsilon_{th} N_t$ and $\tau_{po}=1/\sigma_p \upsilon_{th} N_t$ are respectively the effective lifetimes of electrons and holes in the SCR (τ_{no} and τ_{po} are the *shortest* lifetimes for given N_t and carrier capture cross sections of electrons and holes σ_n and σ_p, respectively [19]); υ_{th} is the charge-carrier thermal velocity; N_t is the concentration of generation–recombination centers. The quantities n_1 and p_1 in Eq. (47) are determined by the ionization energy of the generation–recombination center E_t: $n_1=N_c\exp[-(E_g - E_t)/kT]$ and $p_1=N_v\exp(-E_t/kT)$, where $N_c=2(m_n \kappa T/2\pi\hbar^2)^{3/2}$ and $N_v=2(m_p \kappa T/2\pi\hbar^2)^{3/2}$ are the effective densities of state in the conduction and valence band, m_n and m_p are the effective electron and hole masses, respectively.

The expressions for the electron and hole concentrations in the SCR of Schottky diode involved in Eq. (47) in the chosen reference system take the form [39]

$$n(x,V) = N_v \exp\left[-\frac{E_g - \Delta\mu - \varphi(x,V) - qV}{kT}\right], \tag{48}$$

$$p(x,V) = N_v \exp\left[-\frac{\Delta\mu + \varphi(x,V)}{kT}\right], \tag{49}$$

where $\Delta\mu$ denotes the energy difference between the Fermi level and the top of the valence band in the bulk part of the CIGS layer, $\varphi(x,V)$ is the potential distribution in the SCR at voltage V, given by the expression:

http://dx.doi.org/10.5772/59363

$$\varphi(x,V) = (\varphi_{bi} - qV)\left(1 - \frac{x}{W}\right)^2, \tag{50}$$

φ_{bi} is the height of the potential barrier in equilibrium for holes from the CIGS side related to the built-in (diffusion) voltage V_{bi} by the equality $\varphi_o = qV_{bi}$, W is the width of the SCR given by Eq. (28).

The recombination current density under forward bias and the generation current under reverse bias are found by the integration of $U(x,V)$ throughout the entire depletion layer

$$J = q\int_0^W U(x,V)dx. \tag{51}$$

From the above equations one can obtain the exponential voltage dependence of the recombination current under forward bias.

Substitution of Eqs. (48)–(50) into Eq. (47) and simple manipulation yield the following expression for the generation–recombination rate:

$$U = \frac{n_i(\tau_{no}\tau_{po})^{-1/2}\sinh(qV/2kT)}{\exp(-qV/2kT)\cosh[(E_g^* - 2E_t)/2kT] + \cosh\{[(E_g^* - 2\Delta\mu - qV - 2\varphi(x,V)]/2kT\}}, \tag{52}$$

where $E_g^* = E_g + kT\ln[(\tau_{po}N_c)/(\tau_{no}N_v)]$.

We assume that CIGS contains a lot of shallow and deep impurities (defects) of donor and acceptor types. According to the Shockley-Read-Hall statistics the most effective generation–recombination centers are those whose levels are located near the middle of bandgap. Taking into account this, one can neglect the first term in the denominator of Eq. (52) and obtain the following expression for the current density using Eq. (51):

$$J = qn_i\sinh(qV/2kT)\int_0^W f(x,V)dx. \tag{53}$$

where

$$f(x,V) = \{\cosh[(E_g^* - 2\Delta\mu - qV - 2\varphi(x,V)]/2kT]\}^{-1}. \tag{54}$$

The function $f(x,V)$ has a symmetric bell-shaped form, therefore without incurring noticeable errors, the integration in Eq. (53) may be replaced by the product of the maximum value of the

integrand $f(x,V)$ and its half-width $\Delta x_{1/2}$. By calculating $\Delta x_{1/2}$ as the difference of the values for which $f(x,V)$ is equal to ½, one can obtain under conditions that qV approaches not very close to $E_g - 2\Delta\mu$:

$$\Delta x_{1/2} \approx W\left(\frac{E_g - 2\Delta\mu - qV}{2(\varphi_{bi} - qV)}\right)^{1/2} \cdot \frac{2\,\mathrm{arccosh}2}{E_g - 2\Delta\mu - qV} = W\frac{2kT}{\sqrt{(\varphi_{bi} - qV)(E_g - 2\Delta\mu - qV)}}. \quad (55)$$

So Eq. (53) in the integral form yields the exponential dependence of the recombination current on the applied voltage ($\sinh(qV/2kT)=\exp(qV/2kT)/2$) [37, 38]:

$$J \approx \frac{qn_i W}{\sqrt{\tau_{no}\tau_{po}}} \frac{kT}{\sqrt{(\varphi_{bi} - qV)(E_g - 2\Delta\mu - qV)}}\left[\exp\left(\frac{qV}{2kT}\right) - 1\right]. \quad (56)$$

Fig. 21 shows a comparison of the voltage dependence of the recombination currents in CIGS solar cell, for example, with E_g=1.14 eV calculated using Eq. (51) and (56).

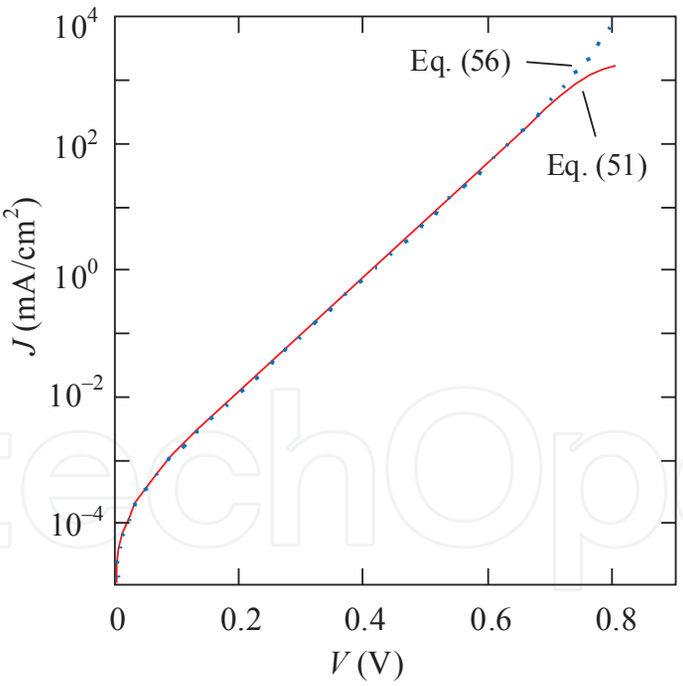

Figure 21. Comparison of the recombination currents in CIGS solar cell with 1.14 eV bandgap calculated from Eqs. (51) and (56).

As seen in Fig. 21, the J–V curves practically coincide. Currents calculated from the exact Eq. (51) exceeds those calculated from Eq. (56) by no more than 5–6% at low voltages and no more than 8–10% at higher voltages. When $V > 0.7$ V the curves are separated from one another

http://dx.doi.org/10.5772/59363

because in deriving Eq. (56) the effect associated with V approaching to φ_{bi}/q did not take into account. Thus, when analyzing the J–V characteristic at higher voltages, only exact Eq. (51) should be applied.

In addition to the results shown in Fig. 21, it is appropriate to draw attention to the rather important fact. If we express the voltage dependence of the recombination current as $J=J_o\exp(qV/AkT)$, the ideality factor A turns out to be slightly different from 2, close to 1.9. It is also appropriate to note that as early as the mid-1990s, the well-known scientists and experts came to the conclusion that the forward current in efficient thin-film CdS/CdTe solar cells is caused by recombination in the SCR of the absorber layer and it was shown that the ideality factor A in these devices coincides with the value 1.9 [40]. Comprehensive analysis and generalization of the experimental results obtained over many years confirm these results [41].

The difference of A from 2 is explained by the fact that according to Eq. (56), the dependence of the recombination current on the voltage is determined not only by the exponent $\exp(qV/2kT)$ but also by the pre-exponential factor $(E_g - 2\Delta\mu - qV)^{-1/2}$, which somewhat accelerates an increase in current with V, and thus lowers the ideality factor.

5.3. Finding the photoelectric characteristics of solar cells

First consider an applicability of the above theory of generation–recombination in the SCR to the experimental data discussed in Section 5.2.

The dark J–V curves (circles) along with the calculated results (solid lines) using Eq. (51) are shown in Fig. 22. In the calculations, we used the exact Eq. (51) in order to reflect the deviation of the forward current from the expression $J \propto \exp(qV/2kT)$, when qV approaches φ_{bi}. For CIS solar cell (E_g=1.04 eV) the experimentally obtained data is shown without modification (shunting is virtually absent), whereas for CIGS with the absorber bandgaps 1.14 and 1.36 eV the presented experimental data is obtained by subtracting the current through the shunts R_{sh} and taking into account the voltage drop across the series resistance R_s. As mentioned previously, at V < 0.1–0.2 V, the values of current under illumination J_{IL} and the short-circuit current J_{sc} are very close to each other, therefore the dark current cannot be determined with a proper accuracy and the experimental points are not shown for low voltages for the three solar cells. For solar cell with bandgap of the absorber E_g=1.5 eV fabricated at elevated temperature the measured data of the dark current is shown for low voltages as well.

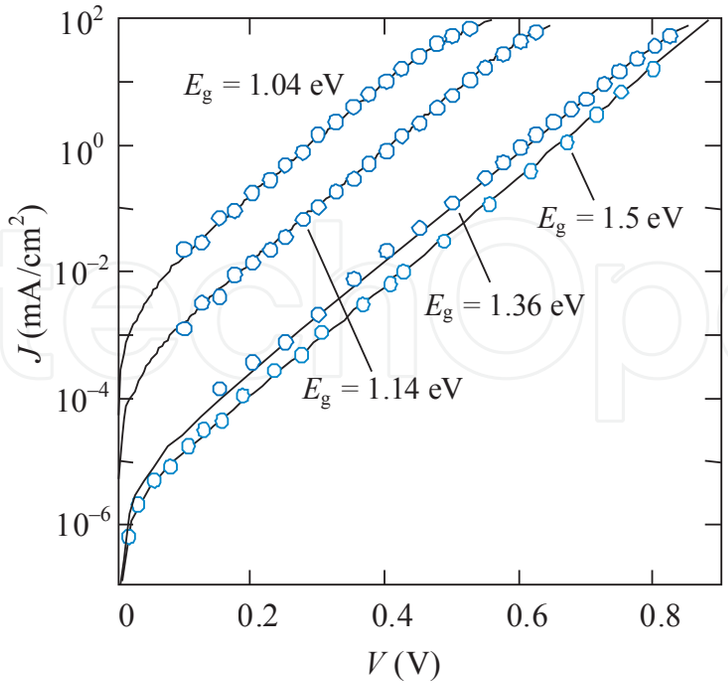

Figure 22. Comparison of the dark forward characteristics of CIGS solar cells extracted from the *J–V* curves under illumination [8] and the generation current (solid lines) calculated from Eq. (51).

As seen in Fig. 22, the calculated results agree well with the experimental data for all solar cells. One point to be mentioned is that in order to obtain a fit with the experimental data of solar cell with E_g=1.5 eV fabricated at elevated temperature, the effective carrier lifetime in the SCR was taken about an order of magnitude less than that for other solar cells. This explains why the curves with so much different bandgaps, E_g=1.36 and 1.5 eV, are located close to each other. It should also be emphasized that reducing the carrier lifetime results in the lowering of open-circuit voltage by ~ 0.06 V, which apparently is one of the negative aspects of the growth and post-growth processing at elevated temperature [36].

Knowing the dark *J–V* characteristics and the short-circuit current densities, it is not difficult to calculate the *J–V* curves under illumination as the dependences of $J_{IL}=J-J_{sc}$ vs. V, which are shown in Fig. 23a by bashed lines. For the short-circuit current densities we use the data given in Fig. 18a, although they can be obtained using the spectral distribution of the quantum efficiency and solar radiation (for the studied samples the discrepancy between the J_{sc} values calculated by these two methods does not exceed 3–4%). Also shown in Fig. 23a by circles are the measured results of the *J–V* curves for the samples with the absorber bandgaps 1.04, 1.14 and 1.36 eV.

Fig. 23b shows the dependences of the electrical power in the solar cell circuit $P=(J-J_{sc})V$ as a function of voltage V. The solid lines in both figures are the calculated results corresponding to the presence of shunts in cells, whereas dashed lines are the results obtained by subtracting the current through the shunt from the measured current.

http://dx.doi.org/10.5772/59363

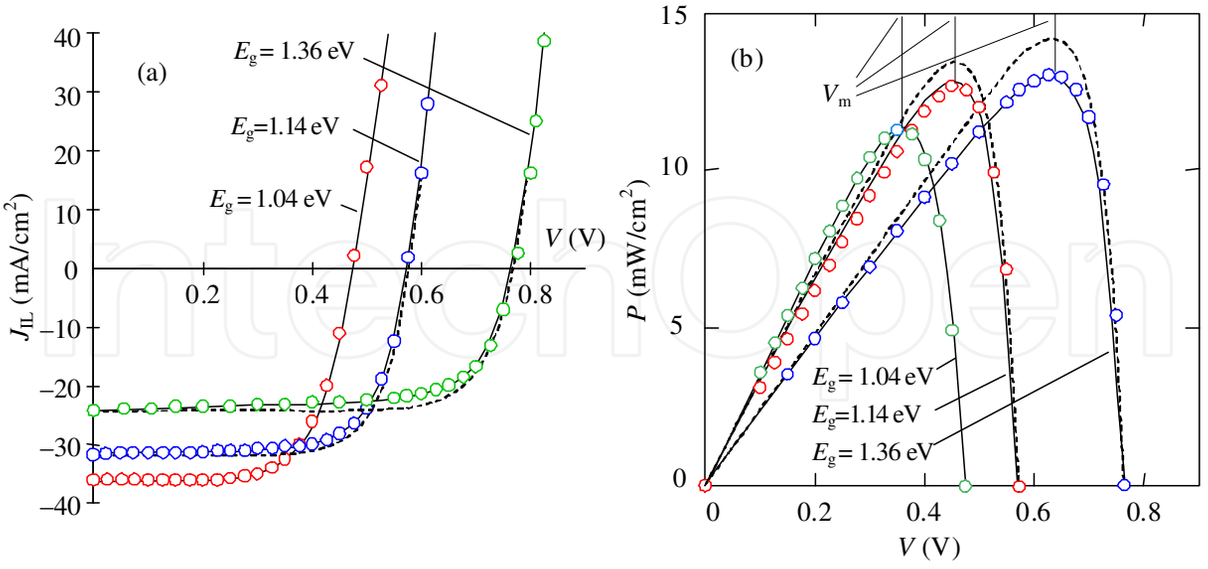

Figure 23. Comparison of voltage dependences of the measured current in CIGS solar cells under illumination I_{IL} (a) [8], and the electrical power P in the circuit of solar cell (b). The measured results are shown by circles, the results of calculations considering the presence of shunts and without them are shown by solid and dashed lines, respectively.

As seen in Fig. 23a, the calculated curve for sample with the bandgap 1.04 eV practically coincides with experimental curve, but in the cases of the absorbers with bandgaps 1.14 and 1.36 eV the calculations give overestimated values of the current. However, if the shunts are taken into account, the calculated and experimental curves for all samples practically coincide. It follows that a comparison of the theory and experiment gives the *quantitative* information on the electrical losses in solar cells. These losses manifest themselves clearly on the voltage dependences of the electrical power P produced by solar cell, $P=(J-J_{sc})V$ shown in Fig. 23b (as in Fig. 23a, the solid lines are the calculated results with the presence of a shunt in cell, whereas dashed line are the results obtained by subtracting the current through the shunts from the measured currents.).

As seen in Fig. 23, the calculated results agree well with the experimental data and indicate a noticeable negative effect of shunting in the studied cells. The effect of shunting is higher when the bandgap of the CIGS absorber is large (shunting does not reveal itself in CIS solar cell). As expected, the shunting does not practically vary the open circuit voltage but reduces the fill factor and the energy conversion efficiency. For the cell with absorber bandgap 1.14 eV, shunting leads to decreasing the fill factor from 0.73 to 0.70 and the efficiency from 13.3 to 12.7%. For cell with the absorber bandgap 1.36 eV, these values are 0.77 to 0.70 and 14.3 to 13.0%, respectively. The fill factor and efficiency of $CuInSe_2$ solar cell are equal to 0.67 and 11.3%, respectively.

Note that the efficiency of studied CIGS solar cells is in the range of 11-14% which is comparable with the efficiency of the modules produced in large volume, but much inferior to record efficiency of small area CIGS solar cells achieved so far.

6. Conclusions

The optical losses in $Cu(In,Ga)Se_2$ solar cells caused by reflections from the interfaces and absorption in the ZnO and CdS layers have been calculated using the optical constants of the materials. When calculating the integral photoelectric characteristics of a solar cell, ignoring the multiple reflections and interference effects in the ZnO and CdS layers cannot cause remarkable errors. (i) The losses due to reflection (reducing the short-circuit current density) from the front surface of ZnO with an antireflection coating in $CuInSe_2$, $CuIn_{0.69}Ga_{0.31}Se_2$ and $CuIn_{0.34}Ga_{0.66}Se_2$ solar cells are equal to 2.5, 1.9 and 1.4%, respectively (antireflection coating increases the photocurrent by 7.1%, 7.4% and 8.0%). The reflection losses at the ZnO/CdS interface are equal to 1.0, 0.9 and 0.9% for these cells, respectively, whereas for the CdS/CIGS interface the losses are 1.3, 1.2 and 1.1%, respectively. The total reflection losses for typical parameters of these solar cells are equal to 4.7, 4.0 and 3.5%, respectively (excluding shading by grid). (ii) The losses caused by absorption in the ZnO and CdS layers amount to 8.1, 7.8 and 9.6% for these solar cells, respectively. The losses due to insufficient absorptivity of the CIGS absorber are 0.6, 0.2 and 0.4%, respectively. The *total optical losses* with the antireflection coating amount to 17.4, 16.0 and 17.5% for solar cells with absorber bandgaps 1.04, 1.14 and 1.36 eV, respectively.

The recombination losses in the studied solar cells have been determined by comparing the measured quantum efficiency spectra with the calculation results. This approach allowed determining the real main parameters of the devices such as: lifetimes of charge carriers, concentration of uncompensated acceptors in the absorber, recombination velocity at the front and back surfaces, the thickness of the CdS film. (i) Recombination at the front surface of the absorber reduces the short-circuit current density by 2.2, 1.9 and 0.2% in solar cells with the CIGS bandgap 1.04, 1.14 and 1.36 eV, respectively. (ii) Recombination in the space-charge region causes a reduction of the short-circuit current density by 0.7, 0.1% and 1.0% for these devices, respectively. (iii) The losses in the neutral part of the absorber and the back surface amount to 2.5, 5.0 and 2.9%, respectively. (iv) Recombination only at the back surface of solar cells cause a decrease in the short-circuit current by no more than 0.2, 1.0 and 0.1%, respectively. *Total recombination losses* in the studied CIGS solar cells with bandgap of absorber 1.04, 1.14 and 1.36 eV are equal to 5.4, 7.0 and 4.1%, respectively. The recombination losses, which degrade the charge collection efficiency of solar cells, can be lowered by increasing the mobility and lifetime of electrons and holes within the literature data. Even greater improvement of the charge collection efficiency can be achieved by extending the SCR. However, positive impact of these measures is limited by the fact that the diffusion length of electrons and the SCR width can become larger than the absorber thickness, which for 100% charge collection efficiency should be increased.

Knowing the short-circuit current density and the dark *J–V* characteristic of $CuIn_{1-x}Ga_xSe_2$ solar cell, the *J–V* curve under illumination can be accurately calculated along with the fill factor, open-circuit voltage and energy conversion efficiency. A comparison of the calculated and measured *J–V* curve under illumination gives the quantitative information on the electrical losses in solar cells indicated a significant impact of shunting, which increases

http://dx.doi.org/10.5772/59363

with increasing the absorber bandgap. If to take into account the effect of shunts, the *J–V* curves of all samples are described by the theory of generation-recombination of charge carriers in the space-charge region. For a cell with the absorber bandgap 1.14 eV, shunting leads to decreasing the fill factor from 0.73 to 0.70 and the efficiency from 13.3 to 12.7%, whereas for cell with the absorber bandgap 1.36 eV the efficiency loss amounts to 1.3%. In $CuInSe_2$ solar cell there are no electric losses, the fill factor and efficiency are equal to 0.67 and 11.3%, respectively. Fabrication technology of CIGS solar cell at elevated temperature (600 – 650°C) allows eliminating the effect of shunting in solar cells with the absorber bandgaps up to 1.4–1.5 eV, but this is accompanied by shortening the carrier lifetime and results in lowering the open-circuit voltage.

Acknowledgements

Author would like to thank Xavier Mathew (Instituto de Energias Renovables, UNAM, Mexico) for his valuable suggestions and support in compiling this chapter.

Author details

Leonid A. Kosyachenko*

Chernivtsi National University, Chernivtsi, Ukraine

References

[1] Bailey S., Raffaelle R. (2011) Space Solar Cells and Arrays. In: Handbook of Photovoltaic Science and Engineering, Luque A. and Hegedus S., editors, 2nd ed. West Sussex, UK: John Wiley & Sons, pp. 365-401.

[2] Green M.A., Emery K., Hishikawa Y., Warta W. (2011) Solar cell efficiency tables (version 37), Prog. Photovolt: Res. Appl. 19: 84-92.

[3] Jackson P., Hariskos D., Wuerz R., Wischmann W. and Powalla M. (2014) Compositional investigation of potassium doped Cu(In,Ga)Se_2 solar cells with efficiencies up to 20.8%. Phys. Status Solidi (RRL) 8: 219–222.

[4] <http://www.pv-magazine.com/services/press-releases/details/beitrag/first-solar-sets-world-record-for-cdte-solar-cell-efficiency_100014340/#axzz2zdlNoCPE>.

[5] < http://www.avancis.de/en/cis-technology/cis-world-records/>

[6] Kosyachenko L.A., Grushko E.V., Mathew X. (2012) Quantitative assessment of optical losses in thin-film CdS/CdTe solar cells, Solar Energy Materials and Solar Cells 96: 231–237.

[7] Kosyachenko L.A., Mathew X., Roshko V.Ya., Grushko E.V. (2013) Optical absorptivity and recombination losses: The limitations imposed by the thickness of absorber layer in CdS/CdTe solar cells, Solar Energy Materials and Solar Cells 114: 179-185.

[8] Shafarman W.N., Siebentritt S. and Stolt L. (2011) Cu(InGa)Se_2 Solar Cells. In: Handbook of Photovoltaic Science and Engineering, Luque A. and Hegedus S., editors, 2nd ed. West Sussex, UK: John Wiley & Sons, pp. 546-599.

[9] Kosyachenko L.A., Mathew X., Paulson P.D., Lytvynenko V.Ya., Maslyanchuk O.L. (2014) Optical and recombination losses in thin-film Cu(In,Ga)Se_2 solar cells. Solar Energy Materials and Solar Cells. 120: 291–302.

[10] Dai Z.-H., Zhang R.-J., Shao J., Chen Y.-M., Zheng Y.-X., Wu J.-D., Chen L.-Y. (2009) Optical properties of zinc-oxide films determined using spectroscopic ellipsometry with various dispersion models. J. Korean Phys. Soc. 55: 1227–1232.

[11] Ninomiya S., Adachi S. (1995) Optical properties of wurtzite CdS. J. Appl. Phys. 78: 1183– 1190.

[12] Paulson P.D., Birkmire R.W., and Shafarman W.N. (2003) Optical characterization of $CuIn_{1-x}Ga_xSe_2$ alloy thin films by spectroscopic ellipsometry. J. Appl. Phys. 94: 879–888.

[13] Bonch-Bruevich V.L. (1970) Interband optical transitions in disordered semiconductors Phys. Status Solidi (b). 42: 35–39.

[14] Born M., Wolf E. (1999) Principles of Optics, 7th ed., Cambridge: University Press, p. 65.

[15] Reference Solar Spectral Irradiance at the Ground at Different Receiving Conditions. Standard of International Organization for Standardization ISO 9845-1:1992.

[16] Wang E.Y., Yu F.T.S., Sims V.L., Brandhorst E.W., Broder J.D., Optimum design of anti-reflection coating for silicon solar cells. 10th IEEE Photovoltaic Specialists Conference. November 13-15, 1973, Palo Alto, California, pp. 168-171.

[17] Pern F.J., L. Mansfield, DeHart C., Glick S.H., Yan F., and Noufi R.. Thickness effect of Al-doped ZnO window layer on damp heat stability of $CuInGaSe_2$ solar cells. Presented at the 37th IEEE Photovoltaic Specialists Conference, Seattle, Washington June 19-24, 2011. Conference Paper NREL/CP-5200-50682.

[18] Kosyachenko L.A., Grushko E.V., Mykytyuk T.I. (2012) Absorptivity of semiconductors used in the production of solar cell panels, Semiconductors. 46: 466-470.

[19] Sah C., Noyce R., Shockley W. (1957) Carrier generation and recombination in p-n junctions and p-n junction characteristics, Proc. IRE 46: 1228–1243.

[20] Schroeder D., Rockett, A, J. (1997) Electronic effects of sodium in epitaxial $CuIn_{1-x}Ga_XSe_2$. Appl. Phys. 82: 4982–4985.

[21] Lavagna M., Pique J.P., Marfaing Y. (1977) Theoretical analysis of the quantum photoelectric yield in shottky diodes. Solid State Electronics 20: 235-242.

[22] Sze S.M., Ng K.K. (2006) Physics of Semiconductor Devices, 3rd ed., New Jersey: Wiley-Interscience.

[23] Brown G., Faifer V., Pudov A., Anikeev S., Bykov E., Contreras M., Wu J. (2010) Determination of the minority carrier diffusion length in compositionally graded Cu(In,Ga)Se_2 solar cells using electron beam induced current. Appl. Phys. Lett. 96: 022104.

[24] Kodigala S.R, (2011) $Cu(In_{1-x}Gax)Se_2$ Based Thin Film Solar Cells. Burlington. USA: Academic Press.

[25] Chien-Chen Diao, Hsin-Hui Kuo, Wen-Cheng Tzou, Yen-Lin Chen, Cheng-Fu Yang. (2014) Fabrication of CIS absorber layers with different thicknesses using a non-vacuum spray coating method, Materials. 7: 206–217.

[26] Dinca S.A., Schiff E.A., Shafarman W.N., Egaas B., Noufi R., Young D.L. (2012) Electron drift-mobility measurements in polycrystalline $CuIn_{1-x}Ga_xSe_2$solar cells, Appl. Phys. Lett. 100: 103901.

[27] Puech K., Zott S., Leo K., Ruckh M., Schock H.-W. (1996) Determination of minority carrier lifetimes in $CuInSe_2$ thin films. Appl. Phys. Appl. Phys. Lett. 69: 3375-3377.

[28] Repins I., Contreras M., Romero M., Yan Y., Metzger W., Li J., Johnston S., Egaas B., DeHart C., Scharf J., McCandless B.E., Noufi R. (2008) Characterization of 19.9%-efficient CIGS absorbers, 33rd IEEE Photovoltaic Specialists Conference, San Diego, California, May 11–16,, Paper NREL/CP-520-42539.

[29] Kosyachenko L., Toyama T. (2014) Current–voltage characteristics and quantum efficiency spectra of efficient thin-film CdS/CdTe solar cells, Solar Energy Materials and Solar Cells 120: 512–520.

[30] Wada T. (1997) Microstructural characterization of high-efficiency Cu(In,Ga)Se_2 solar cells, Solar Energy Materials and Solar Cells 49: 249–260.

[31] Nakada T., Kunioka A. (1999) Direct evidence of Cd diffusion into Cu(In,Ga)Se_2 thin films during chemical-bath deposition process of CdS films, Appl. Phys. Lett. 74: 2444–2446.

[32] Birkmire R.W., Eser E. (1997) Polycrystalline thin film solar cells: Present Status and Future Potential. Annu. Rev. Mater. Sci. 27: 625-53.

[33] Hecht K. (1932) Zum Mechanismus des lichtelektrischen Primärstromes in isolierenden Kristallen, Zeits. Phys. 77: 235-243.

[34] Shafarman W.N., Klenk, W.N., McCandless, R.B.E. (1996) Device and Material Characterization of Cu(InGa)Se_2 Solar Cells with Increasing Band Gap. J. Appl. Phys. 79(9): 7324-7328.

[35] Cooray N.F., Kushiya, K., Fujimaki, A., Sugjyama, I., Miora, T., Okumura, D., Sato, M., Ooshita, M., Yamase, O. (1997) Large area ZnO films optimized for graded bandgap Cu(InGa)Se_2-based thin-film mini-modules. Solar Energy Materials and Solar Cells. 49: 291–297.

[36] Contreras M.A., Mansfield L.M., Egaas B., Li J., Romero M., Noufi R., Rudiger-Voigt E., Mannstadt W. (2012) Wide bandgap Cu(In,Ga)Se_2 solar cells with improved energy conversion efficiency. Progress in Photovoltaics: Research and Applications. 20: 843–850.

[37] Kosyachenko L.A., Maslyanchuk O.L., Motushchuk V.V., Sklyarchuk V.M. (2004) Charge transport generation-recombination mechanism in Au/n-CdZnTe diodes. Solar Energy Materials and Solar Cells. 82(1-2): 65-73.

[38] Kosyachenko L.A. (2006) Problems of efficiency of photoelectric conversion in thin-film CdS/CdTe solar cells. Semiconductors. 40(6): 710-727.

[39] Kosyachenko L.A., Savchuk A.I., Grushko E.V. (2009) Dependence of efficiency of thin-film CdS/CdTe solar cell on parameters of absorber layer and barrier structure. Thin Solid Films. 517: 2386–2391.

[40] Phillips J.E., Birkmire R.W., McCandless B.E., Meyers P.V., Shafarman W.N. (1996) Polycrystalline heterojunction solar cells: A device perspective, Phys Status Solidi B 194: 31–39.

[41] McCandless B.E., Sites J.R. (2011) Cadmium telluride solar cells. In: Handbook of Photovoltaic Science and Engineering. Eds. A. Luque, S. Hegedus, 2nd ed., John Wiley & Sons, Ltd., Hoboken, NJ, pp. 600–641.